Comparison of Jet Quenching Formalisms for a Quark-Gluon Plasma "Brick"

TEC-HQM Collaboration
The Earth, Solar System, Milky Way, Virgo Supercluster, Universe
(Dated: November 16, 2010)

This is the second draft of the outline of a report describing the comparison of various pQCD based formalisms treating the energy loss of hard partons in a thermal quark-gluon plasma for a simplified geometry. Specifically, we compare the predictions of the WHDG and ASW, and Higher Twist (HT) formalisms in the opacity expansion, and of the BDMPS–Z and AMY formalisms in the multiple soft scattering approximation.

I. INTRODUCTION

Jet quenching was among the most spectacular experimental discoveries at the Relativistic Heavy Ion Collider (RHIC). Leading hadrons are suppressed by a factor $4-5$ in central Au+Au collisions at $\sqrt{s_{\rm NN}} = 200$ GeV compared with the expectations from binary collision extrapolated proton-proton collisions at the same energy [1, 2]. Most generally, the notion 'jet quenching' refers to this generic and strong suppression of hadronic spectra, to a class of related jet-like hadron correlations, and to the medium-modification of jets produced by hard parton-parton interactions in highly energetic collisions of large nuclei. Data from the RHIC heavy ion program strongly support the picture that jet quenching is caused by the loss of energy of the primary parton, either by collisions with constituents of the medium (collisional or elastic energy loss [3, 4]) or by gluon bremsstrahlung (radiative or inelastic energy loss [5–7]), prior to hadronization in the vacuum. ~~General arguments dictate that, within the framework of perturbative QCD, the radiative energy loss mechanism dominates over collisional energy loss in the limit of large primary parton momentum.~~ The loss of energy suffered by an energetic quark or gluon penetrating a QCD medium probes dynamical properties of the medium. Therefore, jet quenching is a tool for studying the properties of the hot and dense matter produced in heavy ion collisions.

In recent years, there has been a significant number of efforts to formulate dynamical models of jet quenching and to compare these models to the jet quenching signatures measured at RHIC (see [8? , 9] for reviews). These models make very different assumptions about the dominant physics at RHIC energies; some assume that all interactions are perturbatively weak, some are weak and some strong, and all are strong. Even with the formalisms that assume that the problem is fully approachable within perturbative QCD (pQCD), which we focus on in this paper, there are significant ~~differences in the assumed dominant physics. Comparisons of experimental data to theoretical predictions has not led to the falsification of any one of the perturbative formalisms compared to another. Additionally, direct comparisons of the various pQCD-based models show large~~ quantitative differences between the medium density that is needed to describe the overall suppression of light leading mesons [10? ?]. ~~An elucidation and examination of the theoretical differences and uncertainties underpinning these energy loss models would be extremely useful in determining the root cause of these different density extractions and, in a broader sense, for understanding the properties of the quark gluon plasma produced in heavy ion collisions (HIC). , and to constrain in this way information about medium properties. Direct comparisons of the various models show large quantitative differences between the medium density that is needed to describe the measurements [10].~~ The full modeling of jet quenching in heavy ion collisions contains a large number of steps, such as the initial production spectrum, a time-dependent medium density profile, and fragmentation, which makes it difficult to isolate specific differences between the energy loss formalisms. In this paper, we review the the current state of the art of pQCD-based radiative energy loss models, ~~jet quenching models,~~ including a discussion of their theoretical foundations and limitations, their kinematic region of appliccability, as well as various model-dependent sources of uncertainty. In addition, we provide a systematic quantitative comparison of energy loss formalisms using a specific model problem: the energy loss of light quarks in a medium of constant density, a QGP brick. We will restrict the discussion to leading parton energy loss, for which the largest body of theoretical work exists.

Our report is organized as follows: The first section provides an executive summary of our main findings, with particular emphasis on common features, technical and conceptual differences and uncertainties of different jet quenching models. This section is a self-contained narrative with short introduction to the different classes of jet quenching models. It is written to be easily readable by the generally interested reader. To maintain maximal readability despite the often technical nature of the subject, this executive summary will refer to the following sections for more detailed arguments supporting the main statements. The following sections will then provide detailed explanation and numerical studies of different jet quenching models, and their cross comparison. For more extensive descriptions of the various jet quenching formalisms and of the available phenomenology including model–data comparisons, we refer to the existing reviews [8, 9, 11, 12]

II. EXECUTIVE SUMMARY

A. Jet quenching is caused by parton energy loss

Before discussing how jets and high-p_T hadrons are modified due to the hot and dense QCD matter produced in heavy ion collisions, we shortly recall pertinent features of their production in the absence of medium effects. In elementary collisions (e^+e^- or pp or $p\bar{p}$), our understanding of hadron production at high transverse momentum is relatively mature. Hadron production results from partonic high-momentum transfer processes that can be described with controlled uncertainty as a factorized convolution of incoming parton distribution functions, a hard partonic collision process, and the fragmentation of the partonic final state. In ultra-relativistic heavy ion collisions, there is currently no firm theoretical argument that production cross sections factorize. Rather, factorization is a working assumption that is consistent with phenomenological analyses made so far and that underlies all model studies discussed in this report. General considerations indicate that if factorization is assumed, the hard partonic interaction itself cannot be modified by the medium, since it occurs on temporal and spatial scales too short to be resolved by the medium. However, it is likely that the parton distribution functions in nuclei differ from those in nucleons, and it is possible that the fragmentation of outgoing partons is modified by the presence of the QGP medium.

We know with certainty that jet quenching receives its main contribution on the level of the outgoing fragmenting parton. This follows from several lines of argument. In particular, it is found that the production of direct photons, which have no strong interaction with medium, does not show the large suppressions characteristic for jet quenching. [**?**] ~~This is so for the transverse momentum spectra of photons, and for the transverse momentum spectra of hadrons in deuteron-gold collisions.~~ Moreover, there are by now several global pdf fits that parametrize the nuclear dependence of incoming parton distribution functions (npdfs). For the typical momentum fractions x and virtualities Q relevant for hard processes, these npdf-fits show nuclear modifications of the order of 10-30 % that cannot account for the observed factor 4-5 suppression of single inclusive hadron spectra. [**? ?**] Therefore, the energy degradation observed in nucleus-nucleus collision for all hadronic high transverse momentum spectra must be due to dynamical effects occurring after the hard process ('final state effects').

Furthermore, there is strong experimental evidence that the final state effect responsible for jet quenching is of partonic nature, i.e., that it occurs prior to hadronization. In particular, existing data do not show any evidence that the characteristically different nuclear 'absorption' cross sections of different hadron species play a role in understanding the jet quenching effect. In addition, since hadron formation times are Lorentz dilated in the lab frame **Note:** AM comment: 'I am not sure the following argument is actually relevant for jet quenching, what is more important is that the virtuaqlity be much larger than Λ_{QCD} on exit.' MvL: I guess the question is whether the formation time is determined by pt (momentum) or rather by virtuality. Opinions?, one expects on general grounds that with increasing p_T hadronic effects occur at larger distances from the production point, and should thus be located outside a finite size medium for sufficiently large p_T. That the jet quenching suppression occurs with approximately equal strength for all p_T thus points to a partonic origin of the effect.

As a consequence of these generic observations, all current efforts to understand and simulate jet quenching are based on models of parton energy loss. Further progress then depends on promoting the relation between jet quenching phenomenology and parton energy loss from a qualitative to a more and more quantitative one. To this end, we embark in the following on a critical assessment of current parton energy loss models.

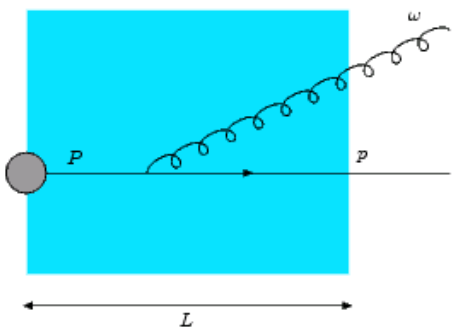

FIG. 1: In a hard parton-parton interactions (denoted by the grey blob), highly energetic partons can be produced. Subsequently, these partons undergo parton branching processes. In a heavy ion collision, this parton evolution occurs within a dense medium (blue area) that interfers with the vacuum evolution via *a priori* unknown elastic or inelastic interactions.

Note: do we need a short discussion on radiative vs elastic e-loss (BM) and non-partonic energy loss (Kopeliovich, Pantuev, Adil-Vitev and non-perturbative AdS etc) (NA) ?

B. Models of radiative parton energy loss

A basic parton branching process within a medium of finite size L is depicted in Fig. 1. Calculations of radiative parton energy loss aim at determining such processes within the framework of perturbative QCD. All approaches studied so far involve significant assumptions and approximations about

- the virtuality and (repeated) branching of the hard parton;

- the nature of the medium through which the energetic parton propagates; and
- kinematical approximations for the interaction between medium and projectile parton.

It will turn out that the root of the largest quantitative differences among the various models lies not so much in differences in their basic underlying assumptions but rather in the details of how the limitations of the common framework, i.e. eikonal propagation and collinearity of radiation, are overcome. **Note:** see WH comments. Needs clarification/better formulation. This is important, so propose some common word-smithing effort. Specifically, this refers to how energy-momentum constraints are implemented, which is of particular importance for large-angle radiation, how multiple gluon emissions are treated, how the medium itself is modeled, and so on.

In the remainder of this Section, we will first provide a short general discussion of in-medium QCD radiation, before describing the specific implementations.

1. *Virtuality and parton branching in the medium*

A high-p_T parton, produced by a hard initial collision between incoming partons, carries initially a high virtuality. Even in the absence of a medium, the parton will undergo 'vacuum' splitting processes to reduce its off-shellness. A typical first parton splitting process after production is sketched in Fig. 1. If occurring in medium, the question arises whether this parton splitting is just the same as in the vacuum, or rather an additional medium-induced splitting, or a result of the interference between medium-induced effects and a dynamics that would also occur in the absence of a medium. None of the existing parton energy loss calculations treats the entire dynamics depicted in Fig. 1 in a field theoretically rigorous fashion. Models of parton energy loss differ in the way in which they interface vacuum splittings and medium effects.

The medium effect on parton splitting is brought about by interactions of the high-energy parton and the radiated gluon with the medium. For small-angle scattering, the parton and the radiated gluon propagate along similar paths, leading to significant interference and a finite formation time of the gluon, which suppresses the gluon radiation compared to incoherent emission. This effect is often referred to as the Landau-Pomeranchuk-Migdal effect. A characteristic consequence of this interference is that the amount of energy loss grows quadratically with L for in-medium path lengths that are small compared to the formation time.

In general, multiple splittings may occur in the medium. A full calculation of multi-gluon final states would include interference terms between the different emitted gluons. However, because such calculations are extremely hard to perform, the current calculations are all based on repeated application of a single-gluon emission calculation. In the following we will separately discuss the single-gluon radiation kernel and the prescription used for multiple gluon emission.

2. *Modeling the medium*

The main interest in studying jet quenching is to use it to characterize the medium through which the projectile parton propagates. In principle, it is of interest to implement different models of the medium in jet quenching calculations, to determine how the medium model and properties affect jet quenching. In the current practice, each model description uses a particular set of simplifications, which can be classified as follows:

1. *The medium is modeled as a collection of static scattering centers*
   In this approach, the medium is modeled as a set of static colored scattering centers with some density distribution along the trajectory of the projectile. A decreasing density can accommodate the physics of an expanding medium. Because gluon radiation from the scattering centers is ignored, calculations in this set-up lead to gauge-invariant (i.e. physically meaningful) results only to leading order in a high-energy approximation. By construction this set-up neglects recoil effects and thus does not allow for elastic parton energy loss.

   This medium model is the basis of two different calculational approaches. The *multiple soft scattering approach* was pioneered by Baier, Dokshitzer, Mueller, Peigné and Schiff [6, 13] (BDMPS) and independently by Zakharov [14]. Gluon radiation is formulated in a path-integral that resums scatterings on multiple static colored scattering centers. Wiedemann [15] showed how this path-integral can be used to include the interference between vacuum and medium-induced radiation. Numerical evaluations of the path-integral employ a saddle point approximation that amounts effectively to assuming that the projectile interacts with the medium via multiple soft scattering processes. In the totally coherent limit, in which the entire medium acts coherently towards gluon production, the BDMPS-Z formalism results in a radiation spectrum that is a radiation term for gluon production with momentum transfer $\mathbf{q}_\perp$ convoluted with a Gaussian elastic scattering cross section $\propto \frac{1}{\hat{q}\,L}\exp\left[-\mathbf{q}_\perp^2/\hat{q}\,L\right]$. In this limit, the medium is fully characterised by the transport coefficient $\hat{q}$, the mean of the squared transverse momentum exchanged per unit path length.

   The *opacity expansion* was pioneered by Gyulassy, Levai and Vitev [16, 17] (GLV) and independently by Wiedemann [15]. It also includes the interference between vacuum and medium-induced radi-

ation and is based on a systematic expansion of the calculation in terms of the number of scatterings. In most existing calculations, only the leading term ($N = 1$) is included, but the behaviour for larger opacities has been explored in [18, 19]. The medium is characterised by two model parameters, the density of scattering centers n or mean free path λ, and a Debye screening mass μ_D used to regulate the infrared behavior of the single scattering cross section. In contrast to the multiple soft scattering approximation, this approach includes the power-law tail of the scattering cross section expected from QCD, leading to shorter formation times of the radiation compared to the multiple-soft scattering approximation [20]. There are several model implementations in the literature that differ significantly in their kinematic approximations. We refer to them as ASW-OE and GLV [or WHDG rad?] [21], and we discuss these differences in detail in Section III B. Extension of the opacity expansion formalism to a medium with dynamical scattering centers was recently explored by Djordjevic and Heinz [22].

2. *The medium is characterized by matrix elements of gauge field operators*
In principle, multiple gluon exchanges between a partonic projectile and a spatially extended medium can be formulated in a field theoretically rigorous fashion by describing the medium in terms of expectation values of 2-, 4-, 6-, 8-, ... field correlation functions. Energy loss calculations based on the higher-twist (HT) approach were pioneered by Guo and Wang [23, 24]. The approach includes the interference between vacuum and medium-induced radiation. Properties of the medium enter the calculation in terms of higher-twist matrix elements. In practice the matrix elements are factorized in the npdf and matrix elements describing the interaction between final state partons and the medium. This factorization is valid at leading order in the path length L in the medium. As we discuss in some detail in section xx, the approximations currently employed result in a formulation of parton energy loss calculations that closely resembles models starting from a set of static scattering centers.

3. *Thermally equilibrated, perturbative medium*
The formulation of parton energy loss within a field-theoretically rigorous defined medium in perfect thermal equilibrium is obviously of great relevance for heavy ion physics. This approach was pioneered by Arnold, Moore and Yaffe [25, 26] (AMY) for a weakly coupled medium. The medium is formulated as a thermal equilibrium state in Hard Thermal Loop improved finite temperature perturbation theory. As a consequence, all properties of the medium are specified fully by its temperature and baryon chemical potential. The calculation does not incorporate vacuum branching of the projectile parton. In principle, the perturbative description of the thermal medium applies only at very high temperature $T \gg T_c$.

As seen from the list above, different models of parton energy loss characterize the medium in terms of different primary model parameters. In the existing literature, the different approximations used for the medium in the various approaches have led to different ways to specify the medium properties. Recently it has become customary to translate the primary model parameters into an effective $\hat{q}$, that has the physical interpretation of an averaged squared momentum transfer between the medium and the fast parton per unit path length $\hat{q} = \langle q_\perp^2 \rangle / \lambda$. This transport coefficient can be calculated from the differential scattering cross section $d\sigma/d^2q_\perp$ in the medium or the rate of momentum exchange, $d\Gamma_{el}/d^2q_\perp$. In this paper, we will use a common approach to calculate $\hat{q}$, using rates from Hard Thermal Loop (HTL) effective field theory. The basic parameters in the opacity expansion are the screening length μ_D and the mean free path λ, which can also be calculated in HTL. For details, we refer the reader to Section III A.

Formally, the Higher Twist (HT) formalism encodes the scattering power of the medium into a nonperturbative matrix element of the gauge field strength tensor $F^a_{\mu\nu}$. In practice, approximations are made, such as neglecting the scale dependence of the matrix element, such that the Higher Twist formalism uses directly the transport coefficient $\hat{q}$.

3. *Kinematic approximations in different parton energy loss models*

With regard to the technical approximations employed in parton energy loss calculations, the four model classes show important commonalities, but display also characteristic differences.

The three main assumptions that are made in all the calculations are

- Both the parton and the radiated gluon (?) are on an eikonal trajectory: the parton energy E is much larger than the transverse momentum exchanged with the medium $q_\perp$, $E \gg q_\perp$ and energy of the emitted gluon ω is also much larger than the exchanged momentum: $\omega \gg q_\perp$.

- Small-angle (collinear) radiation , the energy of the gluon is much larger than its transverse momentum k_T, $\omega \gg k_T$

- Discrete scattering centers, or some form of localised momentum transfer: the mean free path λ is much larger than the Debye screening length $1/\mu$ $\lambda \gg 1/\mu$.

Since the eikonal approximation is used, one often uses the additional approximation that the gluon energy is much smaller than the parton energy $\omega \ll E$, or $x = \omega/E \ll 1$, i.e. the soft radiation approximation.

Let us first consider the kinematic constraints $E \gg \omega \gg k_T, q_\perp$, which is often referred to as the soft eikonal limit. In the calculations, this limit is used for example to neglect the changes to the parent trajectory due to multiple scattering, which simplifies the calculations significantly. In phenomenological applications of parton energy loss, however, gluon radiation is calculated in the entire allowed phase space, up to $\omega = E$ and $k_T = \omega$, where the approximations are not valid. The approximations employed in the current calculations lead to finite radiation probability at the kinematic bounds $\omega \approx E$ and $k_T \approx \omega$, thus violating energy-momentum conservation. Most current formalisms remedy this by imposing explicit cut-offs at the kinematic bounds. The sensitivity of the result to large-x and large angle radiation can be explored to get an impression of the accuracy of the result. The two limits warrant separate discussions.

Consider the large-x regime, where $\omega \approx E$. For all energy loss models, the gluon energy distribution peaks at a "typical" energy (which may be very small). As a result, one can always restrict the considerations (and in most cases the measurement as well) to a reasonably high parton energy for which the calculated rate at $x \to 1$ is small compared to the total rate, thus giving confidence that the impact of the cut-off at $x = 1$ is small. For typical medium densities at RHIC, the gluon energy ω peaks at $O(1$ GeV$)$, so that for parton energies $E \gtrsim 10$ GeV, the probability density at the kinematic boundary becomes reasonably small.

In the present calculational framework, the yield in the spectrum for $\omega > E$, i.e. above the kinematical boundary can be taken as a probability of total absorption of the parton, 'death before arrival'. One alternative would be to simply ignore the probability distribution for $\omega > E$, but this may lead to a situation where the total radiation probability decreases with increasing density or path length, when the typical gluon energy is closer to E. This is clearly not realistic.

The situation is different for large-angle radiation. In the presently existing formalisms, the typical transverse momentum of the radiated gluon k_T depends on the typical transverse momentum exchanges q_T and the number of scatterings L/λ, but not on the gluon energy ω. As a result, there is always some radiation with ω smaller than the typical k_T and thus with a large probability for radiation at $k_T \to \omega$. The quantitative impact of large angle radiation depends on the medium model (large $q_\perp$ contributions in the medium cross section) and the choice of parameters. Already in an early publication it was pointed out that the large-angle regime may be important for phenomenological applications, for example in [27]: " ... the BDMPS–Z formalism is based on the assumption of small transverse gluon momentum $|k_T| \ll \omega$ while we find the main contribution to radiative energy loss for $|k_T| = O(\omega)$. Both features question the validity of the BDMPS–Z formalism ..." A detailed discussion of the effect of large angle radiation in the opacity expansion framework in given in Section III B and in [28].

4. *Multiple gluon emission*

Multiple gluon emission is calculated by repeating the single gluon emission kernel as needed.

The simplest procedure for multiple gluon emission is the Poisson ansatz, where the number of emitted gluons follows a Poisson distribution, with the mean number given by the integral of the gluon emission spectrum, and each gluon has the energy distribution given by the single gluon emission kernel. This procedure is used by GLV and ASW. In most cases relevant to the experimental conditions at RHIC, the mean number of radiation gluons $\langle N_g \rangle > 1$, so that the convolution increases the mean fractional energy loss $\langle \Delta E \rangle / E$ to values larger than the mean value $\langle x \rangle$ from the single emission distribution dN_g/dx. In general, this procedure leads to a distribution of lost energy that does not conserve energy as the degrading momentum of the parent parton is not dynamically updated. However, in most cases, the probability to radiate a larger energy than the incoming parton energy is limited, so that the uncertainty associated with this effect is small. For a more detailed study, see [29].

HT and AMY both use a coupled evolution procedure to calculate multiple gluon emission. In the case of HT, DGLAP evolution is used, which includes the virtuality evolution in vacuum. In the AMY approach, rate equations are used and no vacuum radiation is included.

The evolution equations used in HT and AMY both include the coupling between the quark and gluon distributions in the jets and keep track of the gradual degradation of the jet energy. The emission probability distribution changes as the jet energy degrades, which may seem to be a significant improvement over the Poisson convolution approach. ~~This effect is not included in the Poisson convolution, where the emission probability is calculated with the initial jet energy. In this sense, using evolution equations is a more natural approach.~~ There is, however, an important point that is not explicitly addressed in any of the models: as the energy degrades, the remaining pathlength through the medium also decreases. So, in principle, the energy-evolution should be accompanied by an evolution in coordinate space and the emission probabilities should be calculated using local information about the parton energy, the medium, and the remaining pathlength. This is however difficult in the presence of interference effects, where the gluon radiation is not a purely local phenomenon, but instead couples to the parton over a extended area.

C. Schemes of radiative parton energy loss

Note: Section moved. Used to be directly after the 'modeling the medium section', but now moved here, because it serves as a wrap-up/structuring of the previous discusions. This section may need some more polishing

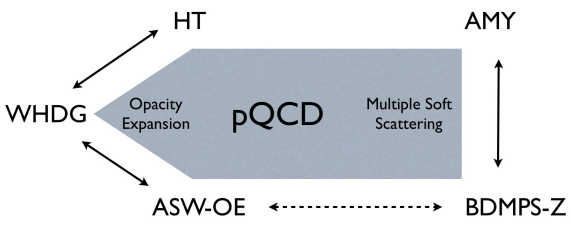

FIG. 2: The landscape of pQCD based jet quenching formalisms. Arrows indicate pairs of formalisms for which detailed analytical and numerical comparisons are presented.

Fig. 2 illustrates the close technical and conceptual relations between the different models of parton energy loss. The similarities and differences can best be discussed in a side-by-side comparison of the most closely related formalisms. ~~Formally, these relations can be summarized as follows~~

1. *Multiple soft scattering vs Opacity expansion*
   Prior to making the multiple soft scattering expansion, the BDMPS-Z path integral can be expanded in opacity. On the level of unintegrated cross sections, the results agree with the opacity expansions discussed here. Calculations based on the opacity expansion do not assume that all momentum transfers are soft, but require additional kinematic assumptions (e.g. definitions of kinematic integration boundaries). **Note:** Not clear what the 'additional kinematic assumptions' in the text are; ASW also implements kinematic boundaries in the BDMPS formalism. Suggest to instead mention the fact that multiple soft takes into account 'all' orders in opacity by default, while the standard opacity expansions use N=1 (but can be extended to higher N). This leads to significant quantitative and qualitative differences between the multiple soft scattering approximation and the opacity expansion.

2. *AMY vs multiple soft scattering approach*
   Parton energy loss within the AMY formalism can be formulated in terms of the same path integral entering the BDMPS-Z formalism. The technical commonalities between both approaches are further elaborated in [20, 30]. The main conceptual difference between the AMY and the BDMPS-Z calculation is the formulation of the medium: a equilibrated high-temperature plasma in AMY versus static scattering centers, with a harmonic oscillator potential in BDMPS. There are also important technical differences, however. Most notably: in AMY a infinite-length medium is used, while BDMPS-Z includes finite-size effects in the emission rates. The effect of these differences is discused in detail in [31]. In addition, the ASW calculation include the effect of large angle cut-off on the radiation. This effect is not taken into account in the standard AMY calculation, but is explored in detail in Section IV below.

3. *Opacity expansions: WHDG vs ASW-OE*
   These opacity expansions calculate the same set of multiple scattering Feynman diagrams within the same high-energy and collinear approximation. However, in extending this result from the kinematic region in which these approximations are valid to the entire phase space open for gluon production, they take different approximations. We shall discuss the resulting significant numerical differences in detail below, since they allow us to illustrate the technical origin of one major source of current theoretical uncertainties.

4. *Higher Twist vs Opacity Expansion*
   The Higher Twist formalisms and the ($N = 1$) Opacity expansion are related in the sense that they are formulated for media where the jet scatters a few times per emission. While both formalisms have extended the theoretical set-up to include multiple scatterings per emission, most comparisons to data still make use of the one scattering per emission approximation. This is referred to as leading order in opacity for GLV scheme and as next to leading twist in the higher twist scheme. The characterization of the medium is also somewhat different as the GLV scheme incorporates the full functional form for scattering off a heavy static scattering center and the HT scheme takes the leading transverse momentum moment of the exchanged transverse momentum distribution. The HT scheme, thus assumes a Gaussian distribution for the exchanged transverse momentum.

   The formalisms differ significantly in the way multiple-gluon emission is treated. The Higher Twist calculation uses DGLAP virtuality evolution, while in the Opacity Expansion, multiple gluon emission is described using Poisson distributed independent emissions (see Section II B 4). The DGLAP evolution used in the HT scheme implies that subsequent radiated gluons are ordered in transverse momenta $k_\perp$ (with the $k_\perp$ of a given radiation serving as the upper bound for the subsequent radiation). There is no such restriction in the GLV scheme and each radiation may explore the limits set by the kinematic bounds.

D. Summary of the main findings

Note: will write introductory paragraph.

1. *Effect of kinematic limits:*
All formalisms make use (to varying extent?) of the soft collinear limit $E \gg \omega \gg k_T$. In phenomenological calculations, we have to extend the calculations into the large-x, $\omega \to E$, and large-angle domain $k_T \to \omega$. For sufficiently large parton energies, the uncertainties associated with the large-x domain seem to be reasonably small (see GLV/ASW-OE section). Large angle radiation, however, is expected to be problematic for all models. This is explored in detail in Section (GLV/ASW-SH section), for the opacity expansions, where the resulting uncertainty is found to be about a factor 2 in the gluon spectra. The resulting uncertainty in R_{AA} is energy-dependent and becomes small at large $p_T \sim xx$ GeV [28]. *Would like to add something about AMY, HT and ASW-MS ?*

2. *Effect of treatment of multiple gluon emission:*
In the existing formalisms, the calculation of the single-gluon emission kernel and the calculation of multiple gluon emission are separate steps. GLV, ASW-SH and ASW-MS use the Poisson ansatz; AMY uses rate equations; and HT uses DGLAP evolution. ~~The simplest procedure for multiple gluon emission is the Poisson ansatz (GLV, ASW-SH and ASW-MS), followed by rate equations (AMY) and the DGLAP evolution (HT).~~ We find that differences between the energy loss formalisms originate at the single-gluon level. It is possible that the differences between the multiple-gluon emission treatment further affect the total energy loss, but we have not investigated this in detail. Inclusive observables, such as leading particle energy loss and the single hadron suppression R_{AA} are unlikely to be sensitive to the details of multiple gluon emission, such as whether the gluons are emitted independently (Poisson ansatz) or in a k_T ordered pattern (DGLAP evolution).

3. *Effect of medium model:*
In most of the current energy loss formalisms, the picture of the medium is intrinsically tied to the approach used in the calculation. As a result, it is not possible to separate the effect of the medium model from assumptions made in the rest of the calculation. For example, the multiple-soft scattering calculation ASW-MS is only analytically feasible in the limit of gaussian broadening, which corresponds to scattering centers with a harmonic oscillator potential. On the other hand, the AMY approach uses a medium based on Hard Thermal Loop field theory with dynamical scattering centers. Futher work is required to systematically compare different medium models.

4. *Effect of including vacuum radiation:*
All formalisms include vacuum radiation to some extent, except AMY. In general, interference between vacuum and medium-induced radiation may locally deplete the radiated gluon distribution. This effect may partially explain the fact that the AMY formalism gives the largest suppression at given T or $\hat{q}$. However, as discussed in Section (AMY-BDMPS), another important effect **Note:** are these really two effects, or the same effect? Maybe relabel 'finite length effects'? See also Björn's suggestion below when comparing AMY to the other formalisms is that the AMY formalism uses a radiation rate that is independent of the position along the path, which leads to a much larger radiation amplitude when the medium length is smaller than or comparable to the formation time. **MvL: What about the other formalisms, can we say more about similarities/differences in the way vacuum radiation is included?** *Schenke: All formalisms include vacuum radiation to some extent, except AMY. The fact that AMY shows the largest suppression in the final comparison is mostly due to lack of vacuum radiation. It is the interference of in-medium and vacuum radiation that leads to the L2 dependence of energy loss during the early stage of the evolution. At later times, or larger L this turns into a linear dependence on L. Because AMY implicitly assumes an infinite medium the L2 behavior is lost. This behavior is studied in detail in [31] using the light cone path integral formalism including finite length effects. The obtained rates show the expected linear dependence on L (which corresponds to the L2 dependence of the energy loss) early in the evolution and approach the AMY result at late times.*

Before we end this Section, we emphasize a common limitation of all formalisms of parton energy loss discussed here: They assume that the hadronization of the leading parton occurs in vacuum. The formalisms describe the interaction of the leading parton with the medium strictly at the partonic level, but do not consider any influence of the medium on the hadronization process or final-state interactions of the produced leading hadron with the medium. This appears to be justifiable for leading hadrons with momentum $p_h \gg m_h$, where m_h is the hadron mass, because the formation time for such a hadron is Lorentz dilated by a factor $p_h/M_h \gg 1$, and thus the formation of the hadron may be assumed to occur far outside the medium. We note that this assumption is not generally satisfied under present conditions of heavy ion collisions at RHIC for baryons and mesons containing heavy quarks.

E. Directions for future work

It is clear from the preceding discussion that the current energy loss calculations have a number of specific weaknesses which may have large quantitative impact on the results. Based on our review of the existing models, we can formulate a number of questions for future work.

Firstly, we recommend to develop calculations with better control of the large angle and large energy radiation. In a realistic calculation, the radiation cross section should naturally go to zero at the kinematic limits $k_T = \omega$ and $\omega = E$. It is most important to control the large-angle behaviour; the large-energy regime can to some extent be avoided by concentrating on high-energy partons/jets. The most natural way to control the large-angle behaviour of the radiation would be to use the full Next-to-Leading Order (NLO) matrix elements for $2 \to 3$ scattering with radiation.

The treatments for multiple gluon radiation should also be further investigated. So far, the treatments are based on incoherent superposition and/or k_T-ordering of the shower *MvL: also angular ordering?* . It is worthwhile to quantitatively investigate deviations from these assumptions. Inclusive observables, such as R_{AA} are likely to be rather insensitive to details of the shower evolution. More differential observables may be more suitable to investigate specific multi-gluon emission scenarios.

UW: Can we formulate a set of minimal requirements for a complete/realistic calculation of radiative energy loss, à la the Snowmass-accord for jet finding?

- Energy and momentum conservations; correct kinematic limits.
- Multi-gluon interference and correlations.
- Treatment of radiative and elastic energy loss on equal terms, i. e. not ad incoherent and independent processes.

NA: I fear a little more theory (how medium-induced multiple emissions break the different orderings in the models; what is the size of the first subleading 1/E corrections,...) should be clear before such requirements can be set. Unless we set some very general rules like it should conserve energy etc.

III. DETAILED COMPARISONS OF MODELS

A. Common definition of medium properties $\hat{q}$, μ and λ

MvL: Not sure where this section should go. The detailed discussion here is a prerequisite for the final comparison in Section B, so we could move it there. However, it would be good to use the definitions outlined here also in the individual sections below. In order to compare different energy loss models the relation of the input parameters with the characteristics of the medium have to be understood. For the multiple soft scattering approximation the calculation of the energy loss depends on the transport coefficient $\hat{q}$ and length L traversed by the parton in the medium. The transport coefficient is defined as the mean momentum kick squared $\langle \mathbf{q}_\perp^2 \rangle$ per mean free path λ:

$$\hat{q} = \rho \int d^2 q_T \, q_T^2 \, \frac{d\sigma}{d^2 q_T} \equiv \int_0^{q_{\max}} d^2 q_\perp \frac{d\Gamma_{el}}{d^2 q_\perp} \mathbf{q}_\perp^2, \tag{1}$$

in which Γ_{el} is the rate for elastic collisions in the plasma, $\mathbf{q}_\perp$ is the transverse momentum imported by the medium to the radiated gluon in such a collision and $q_{\max}$ represents a kinematic ultraviolet cut-off. From this already can be seen that in the multiple soft scattering approximation the momentum kick and the mean free path λ cannot be looked at seperately. The differential scattering cross-section is known in two different energy limits [32]:

$$\frac{d\Gamma_{el}}{d^2 q_\perp} \simeq \frac{C_R}{(2\pi)^2} \times \begin{cases} \frac{g^2 T m_D^2}{\mathbf{q}_\perp^2 (\mathbf{q}_\perp^2 + m_D^2)} & \text{if } |\mathbf{q}_\perp| \ll T \\ \frac{g^4 \mathcal{N}}{\mathbf{q}_\perp^4} & \text{if } |\mathbf{q}_\perp| \gg T, \end{cases} \tag{2}$$

in which T is the temperature of the medium, m_D the Debye mass:

$$m_D^2 = (1 + \frac{1}{6} N_f) g^2 T^2, \tag{3}$$

and $\mathcal{N}$ [32] is the colorless density of the medium:

$$\mathcal{N} = \frac{\zeta(3)}{\zeta(2)} (1 + \frac{1}{4} N_f) T^3. \tag{4}$$

The following expression for the differential scattering cross-section makes the transition from the low energy limit to the high energy limit smooth:

$$\frac{d\Gamma_{el}}{d^2 q_\perp} \simeq \frac{C_R}{(2\pi)^2} \times \frac{g^4 \mathcal{N}}{\mathbf{q}_\perp^2 (\mathbf{q}_\perp^2 + m_D^2)} \tag{5}$$

In the high energy limit this approaches equation 2 and it deviates in the soft region due to the difference in the numerator by 17%. The differential cross-section as function of $q_\perp$ for the different energy limits is shown in Fig. 3. The curves labeled with *Interpolated* correspond to the expression (5) and the curves labeled *Soft* correspond to the low energy limit of Eq. (2).

The calculation of the transport coefficient is now straightforward using Eqs. (1) and (5), and depends on the temperature T of the medium:

$$\hat{q}(T) = \frac{C_R g^4 \mathcal{N}(T)}{4\pi} \ln \left(\frac{q_{\max}^2(T)}{m_D^2(T)} + 1 \right). \tag{6}$$

In the high energy limit the constant in the argument of the logarithm vanishes but in the low energy limit its presence is crucial because otherwise unphysical negative values for $\hat{q}$ are possible. In a realistic medium created in a heavy-ion collision naturally both cases will be present.

The value at which $q_{\max}$ should be chosen is process dependent. In the high energy limit the cross-section describes collisions with static scattering centers

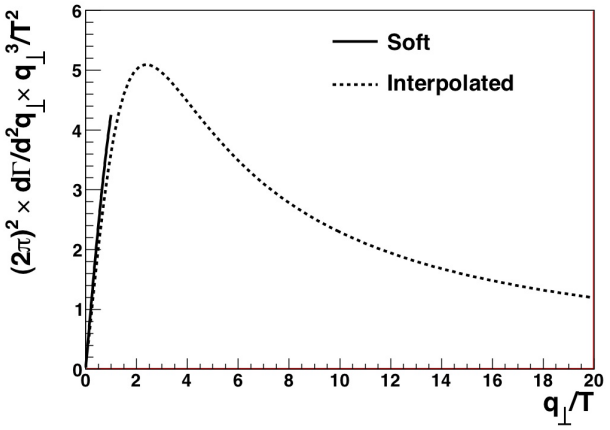

FIG. 3: Differential elastic cross-section as function of $q_\perp$ for the different energy limits. The curves labeled with *Interpolated* correspond to the expression given in Eq. (5). Curves labeled with *Soft* correspond to the low energy limit in Eq. (2).

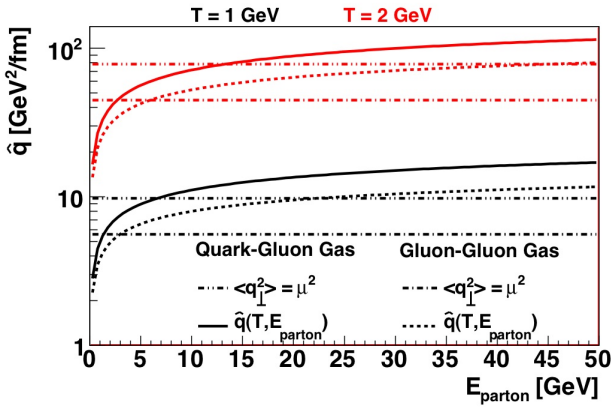

FIG. 4: The transport coefficient as function of the energy of the parton traversing a medium of different tempertures. The transport coefficient is calculated in the hard thermal loop formalism as in equation 6.

as has been argued in [33] and references therein. Therefore in calculations that will follow the upper limit in the integral to calculate $\hat{q}$ in equation 1 will be set at $q_{\max} = g(ET^3)^{1/4}$ which means that $\hat{q}$ not only depends on the temperature T of the medium but also on the energy E of the incoming parton, see Fig. 4. The particles in the plasma are also often approximated as fixed scattering centers by using for the following diffractive scattering cross-section:

$$\frac{d\Gamma_{el}}{d^2q_\perp} \simeq \frac{C_R}{(2\pi)^2} \times \frac{g^4\mathcal{N}}{(\mathbf{q}_\perp^2 + m_D^2)^2}. \tag{7}$$

MvL: N.B. the above uses static scattering centers to calculate lambda; this is identical to what was used in the WHDG paper. Using $1/q_\perp^2/(q_\perp^2+\mu^2)$ for the scattering protential leads to a divergent integral for λ. The Djordjevic-Heinz paper uses $1/\lambda_{dyn} = 3\alpha_s T^3$ – not sure how this was derived, maybe $1/q_\perp^4$ This is done for analytical convenience. In previous work the transport coefficient is often calculated using the approximation $\langle q_\perp^2 \rangle \simeq m_D^2$:

$$\hat{q} \simeq m_D^2 \int_0^\infty d^2q_\perp \frac{d\Gamma_{el}}{d^2q_\perp} = m_D^2\Gamma_{el} = \frac{m_D^2}{\lambda} = \frac{C_R g^4 \mathcal{N}}{4\pi}, \tag{8}$$

in which the scattering cross-section as given in (7) is used. In this case the transport coeffcient does not depend on the energy of the incoming parton. In Fig. 4 for comparison curves for a gluon-gluon and a quark-gluon gas not depending on the energy of the parton are shown as well.

In the opacity expansion formalism the particles in the plasma are also approximated as fixed scatters. This leads to the following expression for the number of scattering centers encountered by the parton traversing the medium:

$$\frac{L}{\lambda} = L \int d^2q_\perp \frac{d\Gamma_{el}}{d^2q_\perp} = 4\pi C_R \mathcal{N} \frac{\alpha_s^2}{m_D^2} L, \tag{9}$$

which is the expression for $\hat{q}$ in equation 8 times L/m_D^2. The number of scattering depends on the temperature of the medium but not on the energy of the incoming parton, note also the horizontal lines in figure 4.

The Higher Twist (HT) formalism encodes the scattering power of the medium into a nonperturbative matrix element of the gauge field strength tensor $F^a_{\mu\nu}$. In light-cone coordinates, this matrix element is given by:

$$\hat{q} = \frac{4\pi C_R \alpha_s}{N_c^2 - 1} \int dy^- \left\langle F^{ai+}(0) F_i^{a+}(y^-) \right\rangle e^{i\xi p^+ y^-}, \tag{10}$$

which measures the transversely acting force due to gluon fields in the medium [34].

B. WHDG and ASW–SH

1. Overview

This subsection contains a detailed comparison of the radiative part of the WHDG calculation [21], equivalent to the first term in the DGLV opacity expansion [35], and the ASW formalism truncated to first order in opacity, here called ASW–SH [36]. We discuss the importance of the definition of the splitting variable x and of the kinematic cut-offs made to enforce the assumptions used in deriving the energy loss formulae. Quantitative results comparing the radiative and elastic components of WHDG will also be shown.

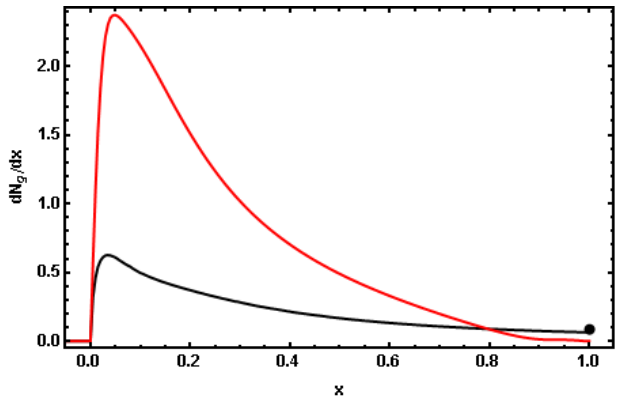

FIG. 5: Plot of the single inclusive gluon radiation distribution, dN_g/dx, from the WHDG implementation of the first order in opacity DGLV formula, Eq. (11), in red, and the ASW–SH implementation of Eq. (12), in black, for a 10 GeV up quark traversing a nominal, 2 fm long static brick of QGP held at a constant $T = 485$ MeV. The point at $x = 1$ indicates the integrated weight of dN_g/dx in the ASW–SH implementation for $x > 1$.

2. *Single emission kernel*

One of the major driving forces of the present investigation was the realization that the approximations and physics assumptions made to arrive at analytical results for the medium-induced radiation not only have an impact on the predictions of experimental observables such as R_{AA} but also influence all the modeling assumptions. An excellent case in point comes when one attempts a naive comparison between the single inclusive gluon distribution implemented in a massless quark and gluon version of the radiative piece of WHDG and the one found from the ASW–SH code [?] for the opacity expansion (see Fig. 1 for a sketch of the perturbative process and definitions of symbols we will use throughout the section). Both purport to compute the single inclusive distribution of gluon radiation, dN_g/dx, to first order in opacity [15–17] for a medium of Debye-screened colored static scattering centers [5]. See Fig. 5, which shows $dN_g^{\rm DGLV}/dx$ and $dN_g^{\rm ASW-SH}/dx$ for a nominal 10 GeV quark jet in a static plasma of length 2 fm and temperature $T = 485$ MeV[62].

The DGLV formula for the first order in opacity energy loss is [35]:

$$x\frac{dN_g^{\rm DGLV}}{dx} = \frac{2C_R\alpha_s}{\pi^3}\frac{L}{\lambda}\int d^2\mathbf{q}d^2\mathbf{k}\frac{\mu^2}{\left(\mathbf{q}^2+\mu^2\right)^2}\frac{\mathbf{k}\cdot\mathbf{q}(\mathbf{k}-\mathbf{q})^2-\beta^2\mathbf{q}\cdot(\mathbf{k}-\mathbf{q})}{\left[(\mathbf{k}-\mathbf{q})^2+\beta^2\right]^2\left(\mathbf{k}^2+\beta^2\right)}\int dz\left[1-\cos\left(\frac{(\mathbf{k}-\mathbf{q})^2+\beta^2}{2xE}z\right)\right]\rho(z). \tag{11}$$

Here m_g and M_q are the effective thermal mass of the radiated gluon and the mass of the parent parton, respectively, $\beta^2 = m_g^2 + x^2M_q^2$, and $\rho(z)$ is the probability distribution for the distance to the first scattering center. (In general one needs to consider the distribution in differences in distance between successive scattering centers. However at first order in opacity there is only one scattering center; as one may always set the initial value of z to 0, $\rho(z)$ is the absolute distance to the first scattering center.) The equivalent expression for ASW–SH, which does not include the effect of a thermal gluon mass m_g, is [37] *NA: find other ref*:

$$\omega\frac{dI^{\rm ASW-SH}}{d\omega} = \frac{2C_R\alpha_s}{\pi^3}\frac{L}{\lambda}\int d^2\mathbf{q}d^2\mathbf{k}\frac{\mu^2}{(\mathbf{q}^2+\mu^2)^2}\frac{\mathbf{k}\cdot\mathbf{q}(\mathbf{k}-\mathbf{q})^2-x^2M_q^2\mathbf{q}\cdot(\mathbf{k}-\mathbf{q})}{\left[(\mathbf{k}-\mathbf{q})^2+x^2M_q^2\right]^2\left(\mathbf{k}^2+x^2M_q^2\right)} \times\int dz\left[1-\cos\left(\frac{(\mathbf{k}-\mathbf{q})^2+x^2M_q^2}{2\omega}\right)\right]\rho(z). \tag{12}$$

If we set $\omega = xE$ in (12) and $m_g = 0$ in β in (11), then we see that Eqs. (11) and (12) are, in fact, identical. Why, then, do the curves obtained by evaluating these expressions, shown in Fig. 5, differ so drastically? The answer lies in the details of the implementation of these two expressions. It turns out that there are a number of choices that must be made in going from the differential expressions for the radiation spectrum to the integrated gluon distribution, dN_g/dx. These are summarized in Table I.

If one alters the radiative energy loss part of WHDG to adopt all the assumptions used in the ASW–SH code, then one finds agreement within numerical precision, as shown in the top left plot of Fig. 6. This corresponds to the choices:

- thermal gluon mass $m_g = 0$;
- thermal quark mass $M_q = 0$;
- use of $k_{\rm max} = xE$ for the maximum allowed value of $k_T = |\mathbf{k}|$;
- use of the same scattering center distribution as in ASW;
- gluon mean free path $\lambda/L = 1$;

	WHDG	ASW–SH
$k_{\max}$	$2x(1-x)E$	xE
x	x_+	$x_{\rm E}$
$q_{\max}$	$\sqrt{3\mu E}$	∞
$\rho(z)$	$2e^{-2z/L}\theta(z)/L$	$\theta(L-z)\theta(z)/L$
L/λ	$L\rho\sigma = L\rho \times 9\pi\alpha_s^2/(2\mu^2)$	1
α_s	0.3	1/3
m_g; M_q	$\mu/\sqrt{2}$; $\mu/2$	0; 0

TABLE I: Table of differences between the implementations of Eqs. (11) and (12) in WHDG and in ASW–SH.

- maximum momentum transfer $q_{\max} = \infty$;
- QCD coupling constant $\alpha_s = 1/3$.

Figs. 6 and 7 show the quantitative progression from exact agreement, when these common choices are made, to the disparate results shown in Fig. 5. The progression systematically removes the changes given in the above list in reverse order.

There are numerous lessons to be learned from Figs. 6 and 7. That the changes in α_s, M_q, and $q_{\max}$ lead to small differences in dN_g/dx is not surprising: α_s differs by only 10% between the implementations; M_q for WHDG is small compared to the jet energy; and it has been known for a long time that dN_g/dx is not sensitive to changes in $q_{\max}$. Also not surprising is the huge difference when L/λ is allowed to vary. While at the level of dN_g/dx one can simply scale the results to account for a varying L/λ, this is not true once the distribution has been folded multiple times into a Poisson convolution; note that the ASW–SH code [**?**] only gives the Poisson convolution results. The differences seen in the dN_g/dx from the two scattering center distributions seems to suggest only a small dependence on their exact form. The apparent huge sensitivity to the inclusion of a radiated gluon mass m_g, however, is a surprise. On the other hand, due to nontrivial interference effects, its effect on observables such as R_{AA} is actually not very large [28].

3. *Definition of the variable x*

The very large changes seen when going from identical to numerically different $k_{\max}$ values (see top right panel of Fig. 7) is a surprise given the assumption of collinearity used in the derivation of the energy loss formulae, Eqs. (11) and (12). This result warrants further explanation. Collinearity, $k_T \ll xE$, is the assumption that radiation is emitted at small angles. To further investigate the meaning of collinearity, it is necessary to discuss the specific definition of the splitting fraction x. As noted in Table I, the GLV-descended derivations [16, 17, 35, 38] interpret $x = x_+ = k^+/P^+$ as the fraction of positive light-cone momentum carried away by the radiated gluon. The ASW–SH derivation [15, 37] defined $x = x_{\rm E} = k^0/P^0$ as the fraction of energy carried away by the radiated gluon. If we denote the usual four-momenta with parentheses and light-cone momenta with brackets then the radiated gluon four-momentum is

$$\begin{aligned} k &= \left(x_{\rm E}E, \sqrt{(x_{\rm E}E)^2 - \mathbf{k}^2}, \mathbf{k}\right) \\ &= \left(x_+E^+, \frac{\mathbf{k}^2}{x_+E^+}, \mathbf{k}\right), \end{aligned} \tag{13}$$

where $\mathbf{k}$ is the momentum of the gluon transverse to the direction of the parent parton and the gluon is assumed to be on mass shell. Similarly, the momentum for a massless parent parton is

$$\begin{aligned} p &= \left((1-x_{\rm E})E, \sqrt{\left((1-x_{\rm E})E\right)^2 - \left(\mathbf{q}-\mathbf{k}\right)^2}, \mathbf{q}-\mathbf{k}\right) \\ &= \left((1-x_+)E^+, \frac{(\mathbf{q}-\mathbf{k})^2}{(1-x_+)E^+}, \mathbf{q}-\mathbf{k}\right), \end{aligned} \tag{14}$$

where $\mathbf{q}$ is the transverse momentum transfer to the parent parton from the scattering center. For completeness the original parent parton momentum is $P = (E, E, \mathbf{0}) = [E^+, 0, \mathbf{0}]$. Using Eqs. (13) and (14) one may derive the exact relationships between x_+ and $x_{\rm E}$:

$$x_+ = \frac{1}{2}x_{\rm E}\left(1 + \sqrt{1 - \left(\frac{k_T}{x_{\rm E}E}\right)^2}\right), \tag{15}$$

$$x_{\rm E} = x_+\left(1 + \left(\frac{k_T}{x_+E^+}\right)^2\right), \tag{16}$$

Note that to lowest order in the expansion parameter is k_T/xE, which controls the extent of collinearity, the two definitions of x are identical.

4. *Collinearity violation and cut-off dependence*

Maybe separate subsection?

A number of simplifying assumptions are made in the process of deriving Eqs. (11) and (12). Specifically, one assumes: (1) eikonality ($E \gg |\mathbf{q}|$); (2) soft radiation ($x \ll 1$); (3) collinearity ($k_T \ll xE$); (4) parent parton pathlength much longer than the mean free path of the gluon in medium ($L \gg \lambda$). The same assumptions are also made in the BDMPS and AMY formalisms [63]. The HT formalism also makes these assumptions, except for (2). It is worth emphasizing that all current pQCD-based energy loss calculations make the assumption of collinearity.

A simple examination of Eqs. (11) and (12) shows that these equations are sensitive to the violation of the assumptions made in their derivation; they do not naturally die out when the approximations used in their derivation break down. As one example, the integrands have support for all k_T. Collinearity has traditionally been enforced through the requirement of forward emission, by

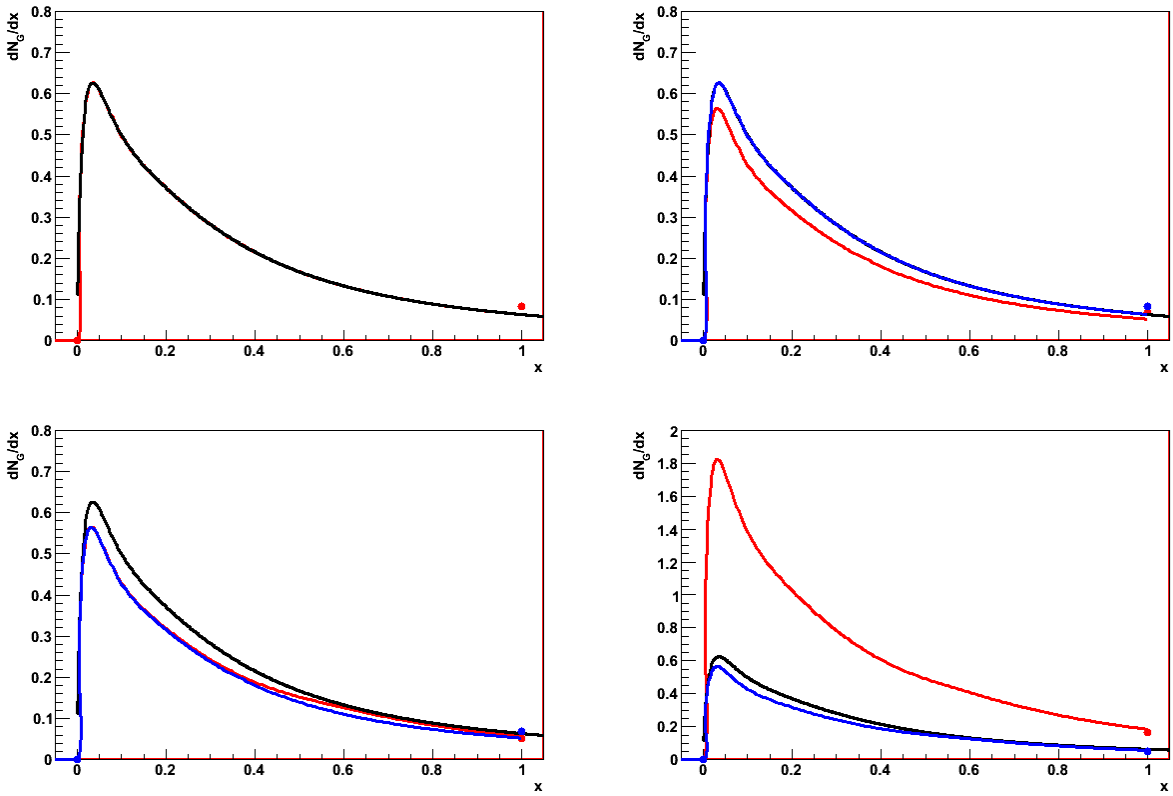

FIG. 6: First half of the progression from ASW–SH to the radiative piece of WHDG. The black curve in all figures represents ASW–SH. The red curve in each figure represents the result when the next progressive change away from WHDG is removed. To aid comparison, the result from the previous plot is shown in blue. Dots at $x = 1$ represent the integrated weight of dN_g/dx for $x > 1$. Progression proceeds as follows: (Top Left) exact reproduction of ASW–SH (within numerical precision); (Top Right) $\alpha_s = 1/3$ to $\alpha_s = 0.3$; (Bottom Left) $q_{\max} = \infty$ to $q_{\max} = \sqrt{3\mu E}$; (Bottom Right) $L/\lambda = 1$ to $L/\lambda = L\rho\sigma = 9\pi\alpha_s^2\rho L/(2\mu^2)$.

cutting off the k_T integration for dN_g/dx in the ultraviolet. In light-cone coordinates forward emission implies that $k^+ > k^-$. This condition implies

$$k_T < k_{\max} = x_+ P^+ = x_+ E^+. \tag{17}$$

In Minkowski coordinates forward emission implies that $k_z > 0$. This condition implies

$$k_T < k_{\max} = x_{\rm E} E. \tag{18}$$

However, requiring forward emission only restricts emission to angles less than 90°, which is still a rather wide angle. One may go further, in anticipation of exploring the sensitivity of results to variations in the k_T cut-off, and define a cut-off angle, $\theta_{\max}$ limiting emission to angles $\theta \leq \theta_{\max}$. This cut-off criterion yields

$$k_{\max} = \begin{cases} x_+ E^+ \tan(\theta_{\max}/2), & x = x_+, \\ x_{\rm E} E \sin(\theta_{\max}), & x = x_{\rm E}. \end{cases} \tag{19}$$

Eqs. (11) and (12) also have support for all values of x. Nonzero weight in dN_g/dx for $x > 1$ of course violates energy-momentum conservation. Requiring the continued forward propagation of the parent parton leads to an additional k_T cut-off that minimally enforces energy-momentum conservation while simultaneously enforcing consistency with the assumption of eikonality. In light-cone coordinates forward propagation implies $p^+ > p^-$; in Minkowski coordinates it implies $k_z > 0$. For the light-cone coordinate case forward emission leads to

$$(1 - x_+)E^+ > |\mathbf{q} - \mathbf{k}| \approx k_T, \tag{20}$$

where $|\mathbf{q}| \sim 3T < q_{\max} = \sqrt{6ET}$ is small compared to most values of $|\mathbf{k}|$; for the Minkowski coordinate case forward emission leads to

$$(1 - x_{\rm E})E > |\mathbf{q} - \mathbf{k}| \approx k_T. \tag{21}$$

For each definition of x there are two cut-offs (e. g. Eqs. (17) and (20) for $x \equiv x_+$ or Eqs. (18) and (21) for $x \equiv x_{\rm E}$); this needs to be taken into account when evaluating the k_T integral over $dN_g/dxdk_T$. One possibility would be to take the minimum of the two definitions; for instance, using light-cone coordinates and taking $\theta_{\max} = \pi/2$; this would mean $k_{\max} = \min(x_+, 1-x_+)E^+$. The present implementations of DGLV and WHDG use a smoother function, $k_{\max} = x_+(1-x_+)E^+$. Note that the

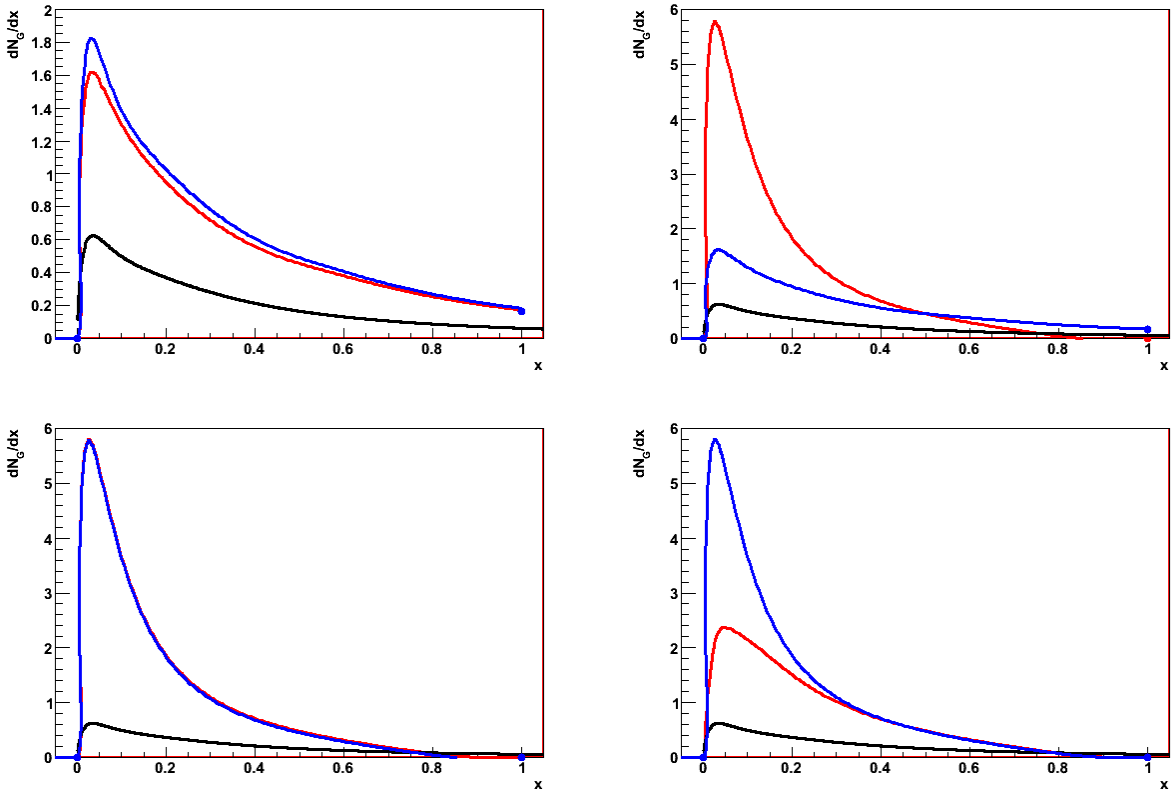

FIG. 7: Second half of the progression from ASW–SH to the radiative piece of WHDG. The black curve in all figures represents ASW–SH. The red curve in each figure represents the result when the next progressive change away from WHDG is removed. To aid comparison, the result from the previous plot is shown in blue. Dots at $x = 1$ represent the integrated weight of dN_g/dx for $x > 1$. Progression proceeds as follows: (Top Left) $\rho(z) = \theta(L-z)\theta(z)/L$ to $\rho(z) = 2e^{-2z/L}\theta(z)/L$; (Top Right) $k_{\max} = xE$ to $k_{\max} = 2x(1-x)E$; (Bottom Left) $M_q = 0$ to $M_q = \mu/2$; (Bottom Right) $m_g = 0$ to $m_g = \mu/\sqrt{2}$.

existing ASW–SH implementation [?] does not include any large-x cut-off.

One could, of course, perform a similar $\theta_{\max}$ analysis for the large-x cut-off. However, one can see from Fig. 8 that the dN_g/dx distribution is actually rather insensitive to this cut-off. In this sense the $dN_g/dxdk_Tdq_T$ integrand respects the small-x approximation rather well.

In order to illustrate the sensitivity of the single gluon emission probability to $k_{\max}$, Fig. 9 plots $dN_g/dxdk_T$ for $x = 0.025$, along with an illustration of three possible cut-offs for k_T:

(a) $x = x_+$ with $\theta_{\max} = \pi/2$;

(b) $x = x_{\rm E}$ with $\theta_{\max} = \pi/2$;

(c) $x = x_{\rm E}$ with $\theta_{\max} = \pi/4$.

Recall that to lowest order in collinearity, the first two cut-offs are identical; the third is a natural $\mathcal{O}(1)$ variation in the cut-off that one can use to estimate the systematic uncertainties deriving from the collinear approximation. Clearly the assumption of collinearity is badly violated: for values of $x \sim \mu/E$, $dN_g/dxdk_T$ reaches its maximum value at $k_T \sim xE$. For these values of x the emis-

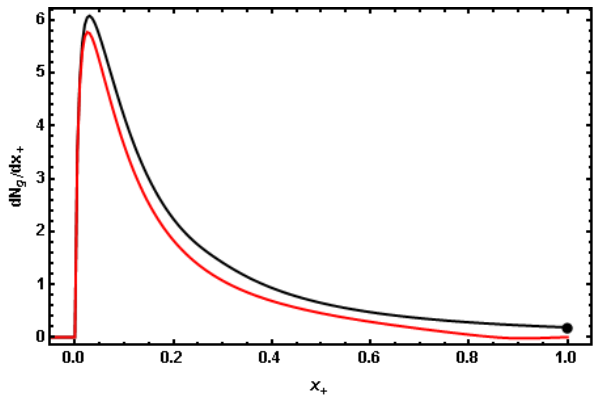

FIG. 8: Plots comparing the result for Eq. (11) with $k_{\max} = x_+E^+$ (black) and $k_{\max} = x_+(1-x_+)E^+$ (red) cut-offs for a 10 GeV up quark traversing a 2 fm static QGP of $T = 485$ MeV. Enforcing the small x approximation, and simultaneously enforcing energy and momentum conservation at the level of dN_g/dx, does not make a large difference to the emission spectrum. The black dot at $x_+ = 1$ represents the integrated weight of dN_g/dx_+ for $x_+ > 1$ when $k_{\max} = x_+E^+$.

sion spectrum is highly sensitive to the choice of $k_{\max}$: $dN_g/dx \sim k_{\max}^2$.

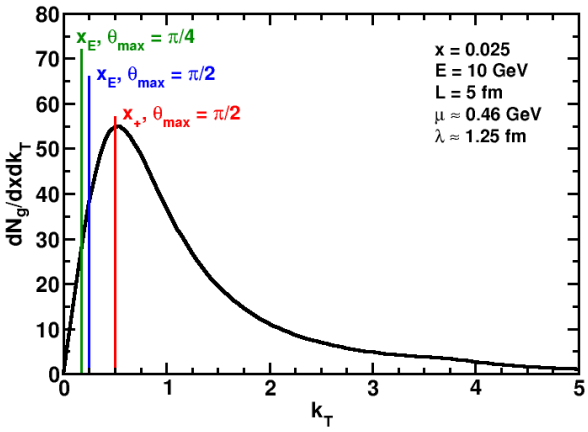

FIG. 9: Plot of $dN_g/dxdk_T$ from Eq. (11) for a light quark with all masses set to 0, $E = 10$ GeV, $L = 5$ fm, and representative values of $\mu \approx 0.46$ GeV and $\lambda \simeq 1.25$ fm for a medium density of $dN_g/dy = 1000$ similar to RHIC conditions [21]. Vertical lines depict the three values of k_T discussed in the text as possible cut-offs to enforce collinearity inEq. (11). Note that with $x = 0.025 \approx \mu/E$, $dN_g/dxdk_T$ is maximized near $k_T \sim k_{\max}$, completely in contradiction to the collinear approximation.

Since the collinear approximation is so badly broken, it is not a good approximation to take $x_+ \approx x_{\rm E}$. A meaningful comparison of results, then, can come only when the emission spectra of Eqs. (11) and (12) are plotted with respect to the same variables. Since one is interested in a differential quantity, a Jacobian is required. We choose to transform x_+ to $x_{\rm E}$ because, ultimately, one is interested in energy loss, as opposed to the loss of positive light-cone momentum. The transformed spectrum is then given by

$$\frac{dN_g^{\rm J}}{dx_{\rm E}}(x_{\rm E}) = \int^{k_{\max}} dk_T \frac{dx_+}{dx_{\rm E}} \frac{dN_g}{dx_+ dk_T}\big(x_+(x_{\rm E})\big), \qquad (22)$$

with

$$\frac{dx_+}{dx_{\rm E}} = \frac{1}{2}\left[1 + \left(1 - \left(\frac{k_T}{x_{\rm E}E}\right)^2\right)^{-1}\right], \qquad (23)$$

$$k_{\max} = x_{\rm E} E \sin(\theta_{\max}). \qquad (24)$$

Note the change in the upper limit (24) of integration in Eq. (22). The resulting comparison of $dN_g/dx_{\rm E}$ is shown in Fig. 10. Note the very large difference in the results for the two collinearly equivalent definitions of x and that for the result with a reduced $\theta_{\max}$. Of course this enormous difference implies very large systematic errors (a factor $2-3$) in the extraction of the medium parameters from leading hadron suppression data [28].

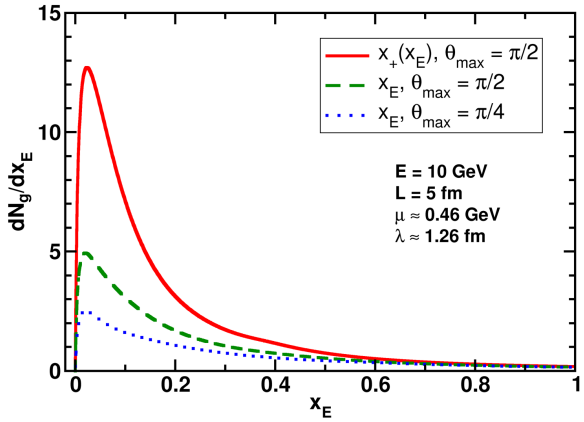

FIG. 10: "Apples-to-apples" comparison of Eqs. (11) and (12) in the massless limit and for which the x_+ dependence of Eq. (11) has been transformed into $x_{\rm E}$; see Eq. (22). Also shown is the result when using the $x_{\rm E}$ interpretation and reducing $\theta_{\max}$ to $\pi/4$, a reasonable $\mathcal{O}(1)$ variation in the k_T cut-off.

5. *Multiple emission*

More explanation necessary?

We finally note that the usual implementation of the Poisson convolution for multiple radiation leads to a distribution that does not conserve energy as the degrading momentum of the parent parton is not dynamically updated. Furthermore, because generally $\langle N_g \rangle > 1$, the convolution almost always pushes the mean fractional energy loss $\langle \epsilon \rangle / E$ to values larger than the mean value $\langle x \rangle$ from the single emission distribution dN_g/dx. Therefore, the Poisson convolution actually enhances the sensitivity of energy loss calculations to regions of larger x for which the approximations are not well controlled.

[**Note from BM:** I do not understand the logic of the last statement. It seems that the collinearity condition is best satisfied for large x. Thus, which "approximations" does the last sentence refer to?]

C. The ASW formalism

As discussed in Section II B 2, the ASW formalism calculates parton energy loss based on a path-integral formalism [15, 37, 39] which can be evaluated either in the multiple soft scattering limit or through an opacity expansion. The GLV $N = 1$ opacity result reproduces our expression [15] on the level of the Feynman diagrams and the analytic expression for the ω- and k_T-differential gluon energy distribution.

1. Energy loss probability distribution

Fig. 11 shows results from the ASW multiple soft scattering limit for different values of a primary quark with energy E and path-length L. All results have been computed with $\alpha_s = 0.3$. First, we plot the probability $P(\Delta E/E)$ — the so-called quenching weight — that a light quark loses a fraction of its energy. The information about $P(\Delta E/E)$ is contained in three pieces:

1. "Untouched survival": This is the discrete probability that a parton does not interact with a medium of length L and that it loses no energy. This probability is represented by a color-coded dot at $\Delta E/E = -0.05$.

2. "Survival with finite energy loss": This is the continuous probability that a parton makes it through a medium of length L but loses a finite fraction $\Delta E/E$ during its passage. This is denoted by the color-coded curve at finite $0 \leq \Delta E/E \leq 1$.

3. "Death before arrival": In general, if one shoots a particle into a wall of thickness L, it can get stopped on its journey before reaching the length L. This probability is denoted by the color-coded dot at $\Delta E/E = 1.05$.

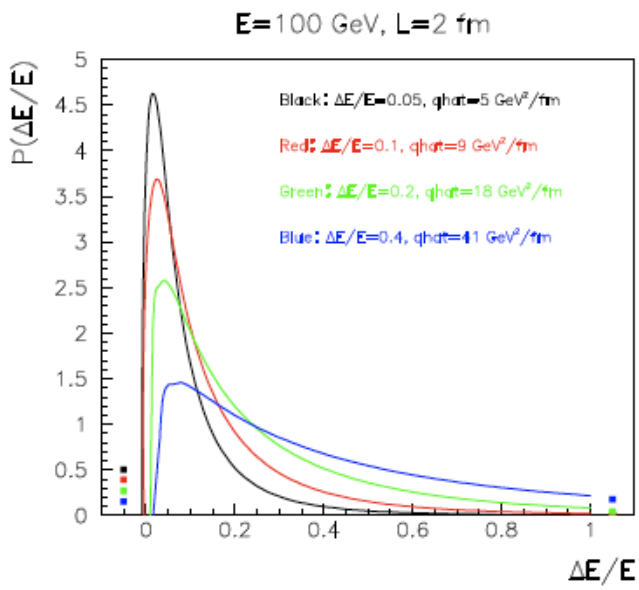

FIG. 11: Probability of energy loss, see the text for explanations, for a light quark of energy $E = 100$ GeV and path length $L = 5$ fm (upper panel) and for a light quark of energy $E = 10$ GeV and path length $L = 2$ fm (lower panel). The legend on the plots indicate the average energy loss and the corresponding value of the transport coefficient $\hat{q}$.

In general, as the average energy loss grows due to an increase in $\hat{q}$, one observes that:

(a) the probability of untouched survival decreases;

(b) the probability of survival with finite energy loss shifts to larger values of $\Delta E/E$;

(c) the probability of death before arrival increases.

This is seen clearly in the plots shown for $P(\Delta E/E)$. The most extreme case is that of $E = 10$ GeV and $L = 2$ fm (lower panel of Fig. 11). Requiring an energy loss of $\Delta E = 4$ GeV in this case amounts to a greater than 40 percent probability of untouched survival but, simultaneously, a 30 percent probability of death before arrival. This comes close to an all-or-nothing scenario, where a particle either goes through without medium modification or gets stuck, but its probability of emergence as an object with reduced energy is relatively small.

2. Gluon radiation spectrum

We now turn to the corresponding spectra: The multiple soft scattering limit suppresses the production of infrared gluons by a destructive interference effect. As a consequence, all spectra are peaked at finite gluon energies. In general, the radiated gluons become harder as one increases the average energy loss (i.e. as one increases $\hat{q}$). If the projectile energy is sufficiently large and the in-medium pathlength is sufficiently small, then the radiated gluons carry small fractions of the projectile energy. This is the case for a projectile quark energy $E = 100$ GeV shown in the upper panel of Fig. 12.

However, if the projectile energy is too small, see lower panel of Fig. 12, one faces a particular problem: One calculates the radiated gluon spectrum as if the parton would propagate through a medium of path-length L, though with finite probability the parton does not have sufficient initial energy to make it through L, and gets stuck before. In the present calculational framework, finding yield in the spectrum for $\omega > E$, i.e., above the kinematical boundary, signals that one has assumed that the particle propagates through a length L though its probability of "death before arrival" is finite.

3. Treatment of kinematic uncertainties

NA: The following could also fit in section II.B.4

The limitations of the high-energy eikonal approximations used in the derivation of the path-integral formalism from which both the multiple soft scattering limit and the opacity expansion stem, were discussed in the original papers [15, 37, 39], together with a comparison of both limits. These limitations and the comparison between both approximations have been recently re-analyzed in much detail in [28]. At this point, let us mention that they were, together with the need of a reliable framework for computing more differential observables like particle correlations or jet shapes, the motivation to include finite energy corrections in the formalism, both at the level of the DGLAP evolution equations [40] or in the form of Monte

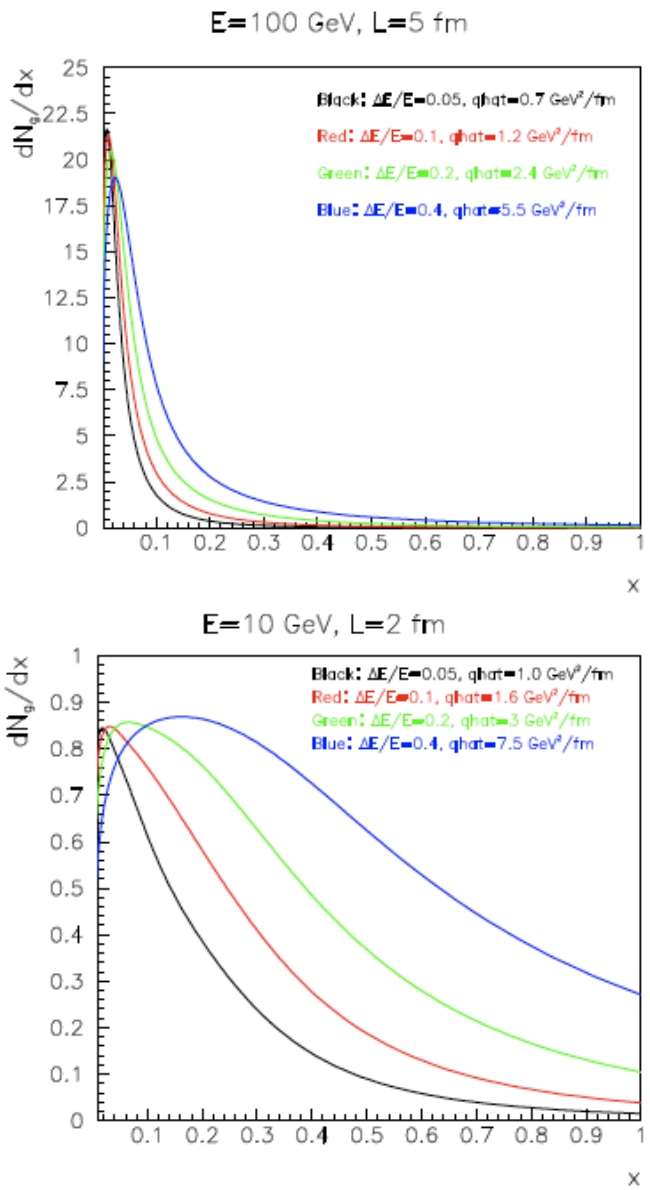

FIG. 12: Energy spectrum of radiated gluons, for a light quark with energy $E = 100$ GeV and path length $L = 5$ fm (top panel) and for a light quark with $E = 10$ GeV and $L = 2$ fm (lower panel). The legends on the plots indicate the average energy loss and the corresponding value of the transport coefficient $\hat{q}$.

Carlo algorithms for final state radiation [41–44]. In this respect, it should be noted that large values of the transport coefficient were required to reproduce RHIC data on single particle suppression [10, 45–49] and back-to-back correlations [47, 49], extracted in analysis using the ASW multiple soft scattering limit through the quenching weights for different models for the medium produced in the collisions. But similar values have been obtained using the mentioned recent developments [40, 43] which do conserve, by construction, energy-momentum both at the one-splitting level and in the parton shower as a whole. This finding confirms the validity of the ASW formalism for phenomenological studies of jet quenching.

D. AMY and BDMPS–Z

1. *AMY transport equations*

The medium-induced radiative energy loss suffered by high energy partons passing through nuclear matter was first computed in BDMPS–Z approach [6, 13, 14, 50, 51], in which the gluon emission probability is expressed in terms of the Green's function of a 2-D Schrödinger equation with an imaginary potential proportional to the cross section of interaction with color center of quark-antiquark-gluon system.

In the AMY approach [25, 26, 52, 53], the gluon emission rates are calculated fully at leading order in α_s by resumming an infinite number of the ladder diagrams in the context of hard thermal loop resummed QCD. Both approaches are valid in the multiple soft scattering limit, but differ in several essential ways: in AMY the medium consists of fully dynamic thermal quarks and gluons, while in BDMPS–Z the medium is treated as a collection of static scattering centers. In BDMPS–Z the gluon emission probability is calculated in the finite configuration space while in AMY the radiation rate is calculated in the momentum space. In addition, different evolution schemes are used: Fokker-Planck equations are solved in AMY to obtain the final parton distributions while in practice BDMPS–Z implementation convolutes the radiation rate with the Poisson distribution to obtain the quenching weights.

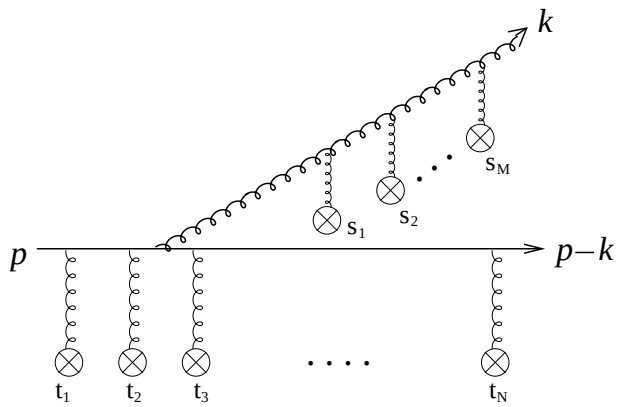

FIG. 13: A typical diagram calculated in the AMY and BDMPS–Z approaches.

The main assumption in these two formalisms is the high enough temperature of the medium such that the asymptotic freedom of the QCD makes it possible to treat the quark-gluon plasma within the perturbation theory. In this case, soft exchanges between the medium and the propagating parton dominates the radiation of a hard

collinear gluon. At the same time, the effect of multiple collisions is reduced due to the coherence between multiple soft scatterings within the formation time of the emitted gluon (LPM effect). This effect makes it necessary to resum all diagrams as depicted in Fig. 13 to calculate the leading order gluon emission probability/rate.

In the AMY approach, one considers a hard parton traversing an extended medium in thermal equilibrium with asymptotically high temperature $T \to \infty$. Due to the small coupling $g \to 0$, a hierarchy of parametrically separated scales $T > gT > g^2T$ makes it possible to construct an effective field theory of soft modes (modes with momentum $|\mathbf{k}| \sim gT$) by summing contributions from hard thermal loops into effective propagators and vertices [54, 55]. The hard parton traversing a thermal QGP undergoes a series of soft elastic scatterings with transverse momentum of order $\sim gT$ off the thermal particles of the medium. The differential cross section (interaction rate) at leading order in α_s is

$$\frac{d\bar{\Gamma}_{\rm el}}{d^2q_\perp} = \frac{1}{(2\pi)^2}\frac{g^2Tm_{\rm D}^2}{\mathbf{q}_\perp^2(\mathbf{q}_\perp^2+m_{\rm D}^2)}\,. \tag{25}$$

Note that the rate has been divided by the quadratic color Casimir C_R of the parent parton, indicated by placing a bar over the rate $\Gamma_{\rm el}$ (similarly for other quantities).

These soft multiple scatterings induce collinear splitting of partons. The time scale over which the parton and emitted gluon overlap is of order $(g^2T)^{-1}$, the same order of magnitude as the mean free time of soft scatterings. To obtain the leading-order gluon emission rates, one must consistently take into account the multiple scattering processes. Within the thermal field theory, one essentially calculates the imaginary parts of an infinite number of gluon self-energy ladder diagrams. The resummation of these ladder diagrams can be organized into the Schwinger-Dyson type equation for the dressed radiation vertex, as depicted in Fig. 14. The corresponding integral equation is

$$\begin{aligned} 2\mathbf{h} \;=\; & i\,\delta E(\mathbf{h},p,k)\mathbf{F}(\mathbf{h}) + \int d^2q_\perp \frac{d\bar{\Gamma}_{\rm el}}{d^2q_\perp} \\ \times\; & \Big[(C_s - C_{\rm A}/2)[\mathbf{F}(\mathbf{h}) - \mathbf{F}(\mathbf{h}-k\,\mathbf{q}_\perp)] \\ & +(C_{\rm A}/2)[\mathbf{F}(\mathbf{h}) - \mathbf{F}(\mathbf{h}+p\,\mathbf{q}_\perp)] \\ & +(C_{\rm A}/2)[\mathbf{F}(\mathbf{h}) - \mathbf{F}(\mathbf{h}-(p-k)\,\mathbf{q}_\perp)]\Big]\,. \end{aligned} \tag{26}$$

In the above equation, δE is the energy difference between the initial and final states,

$$\begin{aligned} \delta E(\mathbf{h},p,k) \;&=\; E_{p-k} + E_k - E_p \\ &=\; \frac{\mathbf{h}^2}{2pk(p-k)} + \frac{m_k^2}{2k} + \frac{m_{p-k}^2}{2(p-k)} - \frac{m_p^2}{2p}, \end{aligned} \tag{27}$$

with p the incoming parton momentum and k the momentum of the radiated hard gluon. $1/\delta E$ is of order of the formation time for the bremsstrahlung process in the medium. The masses appearing in the above equations are the medium induced thermal masses. The 2-D vector $\mathbf{h}$ is the measure of non-collinearity of the final states, defined to be $\mathbf{h} \equiv (\mathbf{p}\times\mathbf{k})\times\mathbf{e}_{||}$, with $\mathbf{e}_{||}$ the chosen longitudinal direction. For the case of $g \to q\bar{q}$, the $(C_s - C_A/2)$ term is the one with $\mathbf{F}(\mathbf{h}-p\,\mathbf{q}_\perp)$ rather than $\mathbf{F}(\mathbf{h}-k\,\mathbf{q}_\perp)$ in the above equation.

The gluon emission rate $d\Gamma(p,k)/dk$ is obtained by closing off the dressed vertex with the bare vertex including the appropriate statistical factors,

$$\frac{d\Gamma(p,k)}{dk} \;=\; \frac{C_s g^2}{16\pi p^7}\frac{1}{1\pm e^{-k/T}}\frac{1}{1\pm e^{-(p-k)/T}} \times \left\{ \begin{array}{ll} \frac{1+(1-x)^2}{x^3(1-x)^2} & q\to qg \\ N_{\rm f}\frac{x^2+(1-x)^2}{x^2(1-x)^2} & g\to q\bar{q} \\ \frac{1+x^4+(1-x)^4}{x^3(1-x)^3} & g\to gg \end{array} \right\} \times \int \frac{d^2h}{(2\pi)^2} 2\mathbf{h}\cdot{\rm Re}\,\mathbf{F}(\mathbf{h},p,k)\,. \tag{28}$$

Here C_s is the quadratic Casimir relevant for the process ($C_F = 4/3$ for quarks or $C_A = 3$ for gluons), and $x \equiv k/p$ is the momentum fraction of the gluon (or the quark, for the case $g \to q\bar{q}$). The subsequent multiple emissions are treated by evolving the momentum distribution $P(p) = dN/dp$ of the traversing hard partons in a set of Fokker-Planck equations,

$$\frac{dP_{q\bar{q}}(p)}{dt} \;=\; \int_k P_{q\bar{q}}(p+k)\frac{d\Gamma_{qg}^q(p+k,k)}{dk} - P_{q\bar{q}}(p)\frac{d\Gamma_{qg}^q(p,k)}{dk} + 2P_g(p+k)\frac{d\Gamma_{q\bar{q}}^g(p+k,k)}{dk}\,, \tag{29}$$

$$\frac{dP_g(p)}{dt} \;=\; \int_k P_{q\bar{q}}(p+k)\frac{d\Gamma_{qg}^q(p+k,p)}{dk} + P_g(p+k)\frac{d\Gamma_{gg}^g(p+k,k)}{dk} - P_g(p)\left(\frac{d\Gamma_{q\bar{q}}^g(p,k)}{dk} + \frac{d\Gamma_{gg}^g(p,k)}{dk}\Theta(k-p/2)\right). \tag{30}$$

In the AMY approach, the medium consists of fully dynamic thermal quarks and gluons; the effect of emitting and absorbing thermal energy are fully included in the evolution equations. In addition, the elastic energy loss due to the recoil of the dynamical scattering centers can also been consistently included in the formalism [56, 57]. However, the transition rates are calculated in momentum space assuming the thermodynamic limit, i.e., the high energy parton experiences a uniform medium on the time scale of the formation time of the emitted radiation.

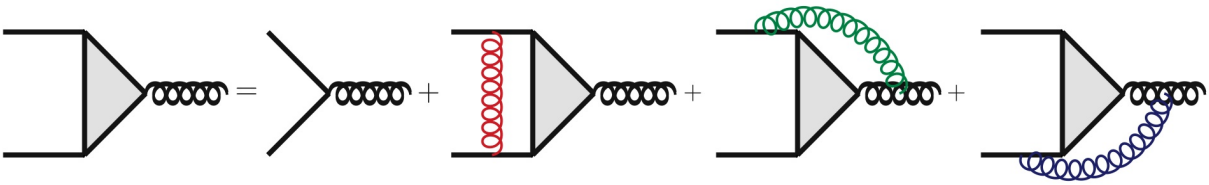

FIG. 14: Diagrammatic representation of the Schwinger-Dyson equation for the emission vertices.

2. *Comparison of BDMPS–Z and AMY*

In the BDMPS–Z formalism, one calculates the amplitude for a quark-antiquark-gluon system evolving in the medium without inducing inelastic reactions (following Zakharov). The general formula for the probability of the gluon emission by a hard parton traversing the medium may be expressed as,

$$k\frac{dI}{dk} = \frac{\alpha x P_{s\to g}(x)}{[x(1-x)p]^2}\mathrm{Re}\int_0^\infty dt_1 \int_{t_1}^\infty dt_2 \Big(\nabla_{\mathbf{b}_1}\cdot\nabla_{\mathbf{b}_2}[G(\mathbf{b}_2,t_2|\mathbf{b}_1,t_1) - G_{\mathrm{vac}}(\mathbf{b}_2,t_2|\mathbf{b}_1,t_1)]\Big)_{\mathbf{b}_1=\mathbf{b}_2=0}. \tag{31}$$

Here I is the probablity of gluon bremsstrahlung from the high energy particle, $P_{s\to g}(x)$ is the vacuum splitting function for relevant process and $G(\mathbf{b}_2,t_2|\mathbf{b}_1,t_1)$ is the Green's function of a 2-D Schrödinger equation with Hamiltonian

$$H(\mathbf{p_b},\mathbf{b},t) = \delta E(\mathbf{p_b}) - i\Gamma_3(\mathbf{b},t)\,. \tag{32}$$

The initial condition for the Green's function is

$$G(\mathbf{b}_2,t|\mathbf{b}_1,t) = \delta^2(\mathbf{b}_2-\mathbf{b}_1). \tag{33}$$

The kinetic term in the Hamiltonian describes the energy difference between initial and final states, as given by Eq.(27), with $\mathbf{p_b} = \mathbf{h}/p$, and Γ_3 in the potential term is the 3-body interaction rate,

$$\begin{aligned}\Gamma_3(\mathbf{b},t) &= \frac{1}{2}C_A\bar{\Gamma}_2(\mathbf{b},t) + (C_s - \frac{1}{2}C_A)\bar{\Gamma}_2(x\mathbf{b},t)\\ &\quad + \frac{1}{2}C_A\bar{\Gamma}_2((1-x)\mathbf{b},t)\,,\end{aligned} \tag{34}$$

where Γ_2 is related to the Fourier transform of the elastic collision rate $d\bar{\Gamma}_{\mathrm{el}}/d^2q_\perp$ by

$$\bar{\Gamma}_2(\mathbf{b},t) = \int d^2q_\perp \frac{d\bar{\Gamma}_{\mathrm{el}}}{d^2q_\perp}\left(1-e^{i\mathbf{b}\cdot\mathbf{q}_\perp}\right)\,. \tag{35}$$

Note that in the original BDMPS–Z formula, the rate $\bar{\Gamma}_{\mathrm{el}}$ for soft scatterings was written as the number density ρ of the static scattering centers in the medium times elastic cross section σ_{el} for such scatterings. Here we follow the notation of Arnold [30] and write BDMPS–Z formulas more generally in terms of the rate $\bar{\Gamma}_{\mathrm{el}}$ for elastic scatterings off the medium constituents. Since the medium is treated as a collection of static scattering centers, one replaces the denominator of Eq. (25) with $(\mathbf{q}_\perp^2 + m_D^2)^2$ for the elastic scattering rate. Further assuming that the gluon emission rate is dominated by the region $b \lesssim 1/m_D$, one may approximate the elastic rate by

$$\bar{\Gamma}_2(\mathbf{b},t) = \frac{1}{4}\hat{\bar{q}}b^2\,, \tag{36}$$

where $\hat{\bar{q}}$ is transverse momentum squared transferred to incident parton per unit time. Neglecting the effective masses of the particles, the Hamiltonian takes the Harmonic oscillator form,

$$H(\mathbf{p_b},\mathbf{b},t) = \frac{p_b^2}{2M} + \frac{1}{2}M\omega_0^2 b^2\,, \tag{37}$$

where

$$\omega_0^2 = -i\frac{(1-x)C_A + x^2C_s}{2M}\hat{\bar{q}}\,, \tag{38}$$

and $M = x(1-x)p$. Making use of the oscillator Green's function and performing the integration over time t_1 and t_2 for a brick of medium with length L, one may obtain the BDMPS–Z formula,

$$k\frac{dI}{dk} = \frac{\alpha x P_{s\to g}(x)}{\pi}\ln|\cos(\omega_0 L)|\,. \tag{39}$$

In practical application, one uses the infinite medium limit of opacity expansion approach [15, 39] to calculate the quenching weights. In the small x limit, the gluon emission probability is independent on the incident parton energy. Then one may convolute with the Poisson distribution to compute the probability $P(\Delta E)$ for the incident parton to lose energy ΔE an incident parton to lose energy ΔE during its passage through the medium [18],

$$P(\Delta E) = \sum_{n=0}^{\infty}\frac{e^{-\langle I\rangle}}{n!}\prod_{i=1}^{n}\left[\int dk_i\frac{dI}{dk_i}\right]\delta(\Delta E - \sum_{i=1}^{n}k_i)\,, \tag{40}$$

where $\langle I \rangle = \int_0^\infty dk(dI/dk)$ is the mean number of radiated gluon for each coherent interaction set. Note the application of Poisson convolution could result in the "leakage" of the probability into the unphysical region where the energy loss by the traversing parton is larger than its initial energy. Practically, this leaked probability is taken as the probability of no energy loss by the incident parton. In contrast, AMY implements exact energy and momentum conservation, both in the elementary process and in the radiative cascade. In addition, the BDMPS–Z approach treats the medium as collection of heavy static scattering centers, therefore elastic energy loss and absorption processes are not present.

Despite these differences, it is worth noting that Arnold has shown [30] that in the multiple soft scattering limit the medium-dependent part for the gluon emission rate from these two approaches are equivalent. Following Arnold [30], we first note that the Green function only depends on the time difference $\Delta t = t_2 - t_1$ due to time invariance. Performing the integral over t_1 which gives a factor of total time, the resulting non-vacuum part of Eq.(31) becomes

$$\begin{aligned} \frac{d\Gamma}{dk} &= \frac{\alpha P_{s\to g}(x)}{x^2(1-x)^2 p^3} \\ &\times \ \mathrm{Re}\int_0^\infty d\Delta t \ [\nabla_{\mathbf{b}_1}\cdot\nabla_{\mathbf{b}_2} G(\mathbf{b}_2,\Delta t|\mathbf{b}_1,0)]_{\mathbf{b}_1=\mathbf{b}_2=0}\,. \end{aligned} \tag{41}$$

One may define the time-integrated amplitude

$$\mathbf{f}(\mathbf{b}) = 2i\int_0^\infty dt[\nabla_{\mathbf{b}_1} G(\mathbf{b},t|\mathbf{b}_1,0)]_{\mathbf{b}_1=0}\,, \tag{42}$$

which satisfies the following equation,

$$-2\nabla_{\mathbf{b}}\delta^2(\mathbf{b}) = H\mathbf{f}(\mathbf{b})\,. \tag{43}$$

In terms of the amplitude $\mathbf{f}(\mathbf{b})$, the gluon emission rate becomes

$$\frac{d\Gamma}{dk} = \frac{\alpha P_{s\to g}(x)}{x^2(1-x)^2 p^3}\mathrm{Re}[(2i)^{-1}\nabla_{\mathbf{b}}\cdot\mathbf{f}(\mathbf{b})]_{\mathbf{b}=0}\,. \tag{44}$$

Fourier transforming Eq. (43) from impact parameter space to momentum space with the use of Eq.(37), one obtains the linear integral equation [Eq.(26)], with $\mathbf{F}(\mathbf{h}) = p\mathbf{f}(\mathbf{p_b})$. The gluon emission rate becomes

$$\frac{d\Gamma}{dk} = \frac{\alpha P_{s\to g}(x)}{4x^2(1-x)^2 p^7}\int\frac{d^2h}{(2\pi)^2}\mathrm{Re}[2\mathbf{h}\cdot\mathbf{F}(\mathbf{h})]\,. \tag{45}$$

Including the appropriate final state statistical factors, one reproduces the AMY formula (28) for the gluon emission rate (see Appendix for further details).

IV. LARGE ANGLE RADIATION IN AMY

In order to explicitly exclude large angle radiation, which is automatically suppressed for $g \ll 1$ but can contribute for larger g, we suppress the large angle contributions in the integral over $\mathbf{h}$ in Eq. (**reference to AMY rate with h integral**) by introducing an envelope function $W(k_\perp, k_{\perp\max})$, where $k_\perp = h/p$.

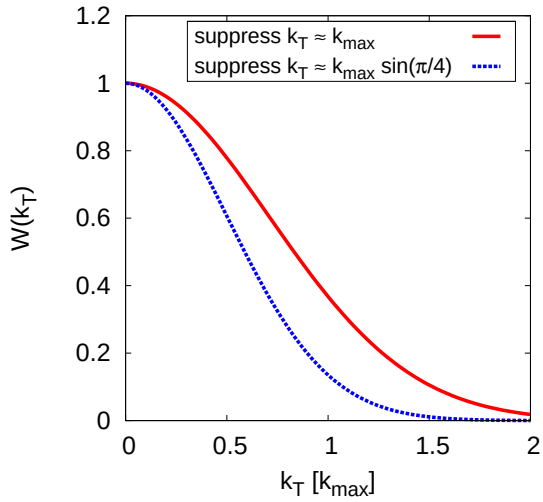

FIG. 15: (Color online) Envelope function W for different maximal transverse momenta.

A reasonable choice for W is a Gaussian that cuts off k_T above a value $k_{\perp\max}$. We choose a Gaussian because the integral equation (**reference to AMY integral equation**) is solved by Fourier transforming into the so called impact parameter space (see [**?**]), where it becomes a differential equation. Hence, we want an envelope function whose Fourier transform is analytic and well behaved. Explicitly we define

$$W(k_\perp, k_{\perp\max}) = \exp(k_\perp^2/k_{\perp\max}^2)\,, \tag{46}$$

where we can vary $k_{\perp\max}$, depending on how much we want to restrict the emission angle. First, we would like to exclude the $k_\perp$ that are kinematically disallowed, so we choose the following $k_{\perp\max}$:

$$k_{\perp\max}^2 = \begin{cases} k^2 & \text{for } |p|>|k| \text{ and } |p-k|>k \\ (p-k)^2 & \text{for } |p|>|k| \text{ and } |p-k|<k \\ (p-k)^2 & \text{for } |p|<|k| \text{ and } |p|>|p-k| \\ p^2 & \text{for } |p|<|k| \text{ and } |p|<|p-k| \end{cases} \tag{47}$$

This suppressed most of the kinematically disallowed $k_\perp$ and makes sure that $k_\perp$ is always smaller than the smallest momentum. Note again, that in the limit of $g \ll 1$ those kinematically disallowed transverse momenta are already suppressed, so that the formalism is perfectly consistent with kinemtatics in the limit where it is derived.

To also suppress k_T, which correspond to emission angles larger than a certain $\theta_{\max}$, we can replace $k_{\perp\max}$ by

$k_{\perp\max}\sin(\theta_{\max})$. Fig. 15 shows the envelope function W for the original $k_{\perp\max}$ and for a maximal emission angle of $\theta_{\max} = \pi/4$. Using a Gaussian, not all contributions from $k_\perp > k_{\perp\max}$ are removed but they are sufficiently suppressed to give a good estimate of the effect of removing these contributions.

3. *Modified rates*

We demonstrate the effect of suppressing large transverse momentum emissions by showing the ratio of the rate including the suppressing envelope and the original AMY rate in Figs. 16 and 17 as a function of k, the absolute value of the three-momentum of the emitted gluon.

For a typical α_s of 0.3, the suppression around small k is significant but decreases for larger k. As expected, the effect is also reduced as α_s decreases, as can be seen in the result for $\alpha_s = 0.01$.

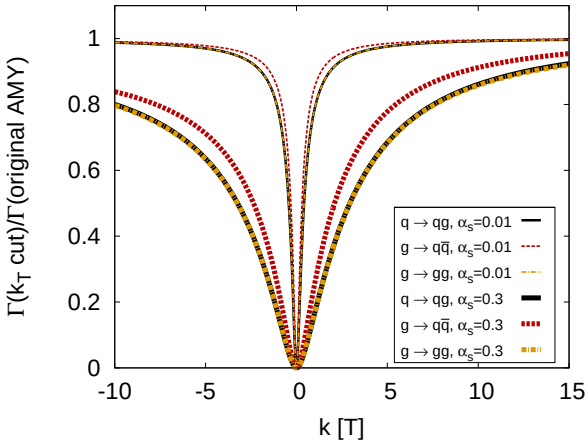

FIG. 16: (Color online) Ratio of the rate for the process $q \to qg$ including the suppressing envelope function and the original AMY rate for two different α_s. $p = 40\,T$.

APPENDIX A: AMY VS. BDMPS–Z

Discussed at INT: some of this should be moved back into the main text About the connection between AMY and BDMPS–Z, the starting point is Eq. (31). The connection between (45) and (39) is not that obvious since in (45) the rate is used and written in momentum space with infinite medium length limit taken, while (39) is written in coordinate space for a finite medium length. To go from probability to rate, one may apply the large-L limit of Eq. (39),

$$\ln|\cos\omega_0 L| \sim |\omega_0| L/\sqrt{2}, \tag{A1}$$

and move L to the left-hand side. Although (45) is written in momentum space, it is just the Fourier transform of

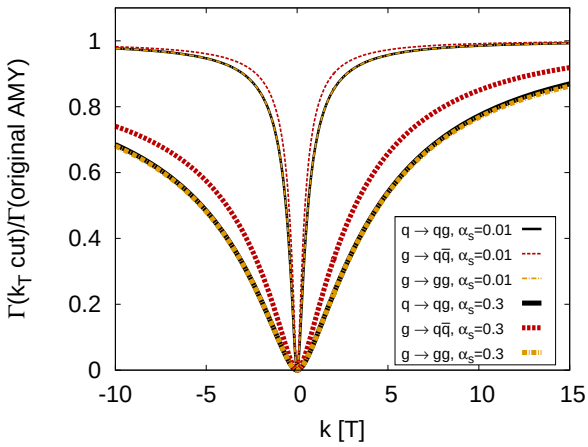

FIG. 17: (Color online) Ratio of the rate for the process $q \to qg$ suppressing emission angles larger than $\pi/4$ and the original AMY rate for two different α_s. $p = 40\,T$.

(44), with the redefinition of $F(h)$, which gives p^7 from p^3. Equation (44) can be directly related to our starting point (31), with a new definition of $f(b)$ in terms of the Green function, so the factor $1/x^2(1-x)^2/p^2$ from Eq. (31) still survives. Note $\omega = k = xp$ has been inserted on the right- hand side of (44), thus x in $xP(x)$ gets canceled and there is an extra p in the denominator. In fact,

$$\mathrm{Re}[(2i)^{-1}\nabla_b \cdot f(b)]_{b=0} \tag{A2}$$

or $\int d^h Re[2h \cdot F(h)]$ with the above mentioned extra factors in Eqs. (44) and (45) correspond to $\ln|\cos(\omega_0 L)|/L$ in Eq. (39). Although it is not a single-step calculation from (31) to (39), the cancellation of this extra factor can be easily understood by noting that the Green function of the hamonic oscillator is dependent on the mass $M = x(1-x)p$, and finally the factor $M^2 = x^2(1-x)^2p^2$ comes out of the expression

$$[\nabla_{b_2}\nabla_{b_1} G(b,t|b_1,t_1)]_{b_1=0,b_2=0}. \tag{A3}$$

Finally performing the time integrations, one arrives at Eq. (39).

APPENDIX B: SYSTEMATIC COMPARISONS

1. Considered energy loss models

In this section, the multiple-soft scattering approximation is compared with the opacity expansion formalism and the McGill AMY implementation. Specifically, the following energy loss models are compared:

- BDMPS–Z/ASW–MS as reported in reference [39].

- ASW-SH: The single hard scattering approximation as described in [39]. It consists of an incoherent superposition of a few single hard scatterings. Originally with a fixed value for L/λ. For this work L/λ is calculated from the temperature T in the medium. Single gluon distribution is an analytical expression as given in Eq. (12).

- WHDG radiative [21]: This model is based on the GLV opacity expansion [16] and calculates the radiated gluon energy starting from an analytical expression for the single gluon emission spectrum to all orders of opacity as given in Eq. (11). For the single gluon spectrum there is a smooth cut-off given by the parton energy. Using the average number of emitted gluons the $P(\Delta E)$ is calculated for a parton. The energy loss is calculated following the DGLV formulas for radiative energy loss as reported in appendix B of [21].

- AMY radiative: The AMY formalism based on a thermal effective field theory approach is described in section III D. In the results shown in this section, the gluon splitting process, $g \to gg$, is neglected.

2. Suppression factor in a QGP Brick

The measured hadron spectra at RHIC follow a power law: $dN/dp_t \sim p_T^{-n}$. If the energy of each hadron is reduced by a fraction ϵ, the hadron spectrum after energy loss will be:

$$\frac{dN}{dp_T} = \frac{1}{[(1-\epsilon)p_T]^n}\frac{dp_T}{dp'_T} = \frac{1}{(1-\epsilon)^{n-1}p_T^n}, \tag{B1}$$

where p'_T is the momentum of the hadron after radiating energy in the medium. Given the probability distribution of energy loss ϵ the nuclear modification factor R_{AA} can be approximated by the weighted average energy loss:

$$R_n = \int_0^1 d\epsilon (1-\epsilon)^{n-1} P(\epsilon), \tag{B2}$$

in which $\epsilon = \Delta E/E$. Because for RHIC energies the hadron p_T spectrum is approximated by a power law spectrum with $n = 6.5$ for $p_T > 2.$ GeV/c [58], R_7 will be used as a proxy for R_{AA}.

a. *Comparison at fixed temperature*

The different energy loss formalisms do not result in the same suppression at equal density. This is illustrated in figure 18(b) where the outgoing quark spectrum is shown for all the models with a medium temperature $T = 300$ MeV. The distributions are given for two different bricks in which the incoming quark has initially $E = 20$GeV. The bricks consist of a gluon gas, $N_f = 0$, of length $L = 2$ fm (left panel) and $L = 5$ fm (right panel). The input parameters to calculate the energy loss in the different models depend on T and L. The corresponding suppression factors R_7 are different while the distributions have a similar shape.

The outgoing quark spectrum is calculated using a Poisson convolution of the single gluon spectrum for the multiple soft scattering approximation and the opacity expansions. This gives a finite probability to the parton to not have any interaction with the medium which given by the squares at $z_{\rm E} = 1$. In this case the parton does not lose any energy. At the same medium density this weight is roughly twice as large for the multiple soft scattering approximation as for the opacity expansions for a brick of $L = 5$ fm, cf. the right panel of figure 18. On the other hand, the gluons that are radiated are softer for the opacity expansions than for ASW–MS. For a brick of $L = 2$ fm and a temperature of $T = 300$ MeV the parton hardly loses any energy in all models, $R_7 > 0.8$ for all models, and the picture is dominated by the very large discrete weights.

In the left panel of figure 18 the single gluon energy spectra are shown. For ASW–MS and ASW–SH the thermal quark and gluon mass are set to zero while in WHDG radiative those masses are included. Including the thermal masses results in less soft gluon radiation which can be seen comparing the ASW–SH and WHDG radiative curves at small ω. Another difference as discussed in Section III B is the cut-off $k_{\rm max}$ on the energy transfer to the gluon. For ASW–MS and ASW–SH it is possible that a radiated gluon has larger momentum than the initial energy of the incoming quark because there is no kinematical bound on the transferred energy ω the gluon is carrying away.

The only kinematical constraint in ASW–MS and ASW–SH is the dimensionless parameter $R(\bar{R})$ constraining $k_T < \omega$ which prohibits large angle radiation but there is no dependence on the energy of the parton. At small x the kinematical boundary $k_T < \omega$ is important while at large x the important constraint is $\omega < E$. In the WHDG radiative formalism this is regulated by an additional kinematical bound which prevends the parton from going backward in case the transferred energy fraction is large $x > 0.5$. This corresponds with the second upper limit in the GLV energy loss formalism [17]: $k^2_{\rm max} = {\rm Min}\,[4E^2x^2, 4E^2x(1-x)]$, which in WHDG radiative is implemented as $k_{\rm max} = 2Ex(1-x)$. So there is a factor 2 difference in the cut-off at small x which results in more soft gluon radiation for WHDG. This is not observed in Fig. 18(a) because of the earlier mentioned difference in the inclusion of mass of the quark and gluon.

b. *Suppression at fixed transport coefficient $\hat{q}$*

Figure 19 shows the dependence between suppression factor R_7 on $\hat{q}$ given by Eq. (6). From this figure can be seen that both opacity expansion formalisms lose

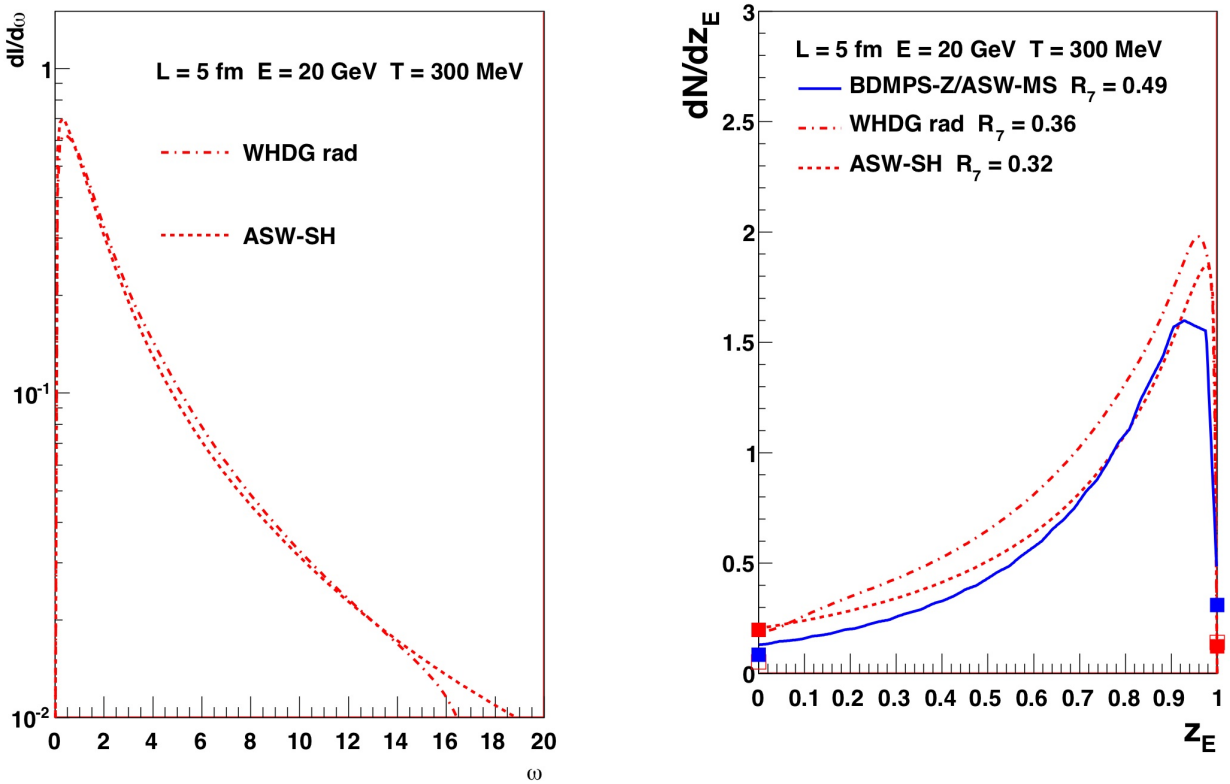

(a) (Single) Gluon Distribution

(b) Outgoing quark Spectrum

FIG. 18: The (single) gluon distribution and final quark energy spectrum as function of $z_E = 1 - \epsilon$. All models have the same input temperature $T = 300$ MeV. The squares at $z_E = 0$ indicate the probability that a quark is absorbed and at $z_E = 1$ the probability that a quark does not interact with the medium. Solid blue squares: BDMPS–Z/ASW–MS. Open red squares: WHDG radiative. Solid red squares: ASW–SH.

more energy at the same medium density (same $\hat{q}$) compared to the multiple soft scattering approximation. The AMY formalism generates more energy loss compared to all the other models at the same medium density. To reach a similar suppression as measured at RHIC [59–61], $R_7 \approx 0.25$, the required densities for the different models differ up to a factor 9 in $\hat{q}$. For a brick of $L = 2$ fm $R_7 \approx 0.25$ is reached at $\hat{q} = 17.8$ GeV^2/fm for WHDG versus $\hat{q} = 8.86$ GeV^2/fm for ASW–SH while the the multiple-soft scattering approximation needs $\hat{q} = 23.2$ GeV^2/fm to reach the same suppression. In the AMY formalism only $\hat{q} = 2.7$ GeV^2/fm is required. For a brick of $L = 5$ fm the required values are $\hat{q} = 0.4, 0.95, 1.23$, and 2.11 GeV^2/fm, respectively, for AMY radiative, ASW–SH, WHDG radiative and ASW–MS for a suppression factor $R_7 = 0.25$.

In Tables II and III different characterics like input variables and gluon densities of all the considered energy loss models are listed. The larger energy loss in the opacity expansion formalism than for ASW–MS is mainly caused by the smaller discrete weights of the energy loss probability distribution under the same medium conditions. In the AMY formalism an infinite medium is assumed which removes the destructive interference of the vacuum radiation with the medium induced gluon radiation resulting in much larger energy loss under the same medium conditions. In the AMY formalism there is no interference with the vacuum radiation implemented at all because it does not exist for an infinite long medium.

c. *Comparison at fixed suppression R_7*

In Fig. 20 the inclusive gluon spectra for the bricks of different length are shown. These spectra correspond to a suppression factor $R_7 = 0.25$, corresponding to the medium densities reported in TableII and shown Fig. 19. The single gluon spectrum WHDG does not have a tail because in the WHDG calculation the single gluon spectrum is modified by a factor which smoothly cuts off the spectrum at the energy of the incoming quark $E = 20$ GeV. For the AMY gluon spectrum only $q \to q + g$ split-

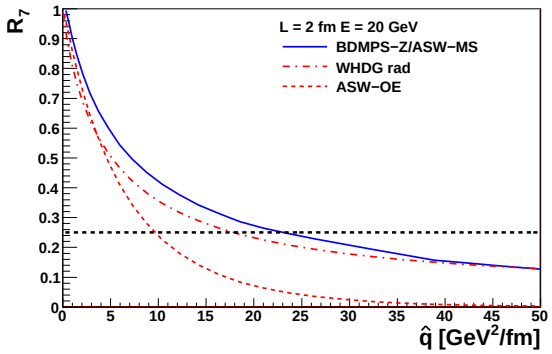

(a) $L = 2$ fm.

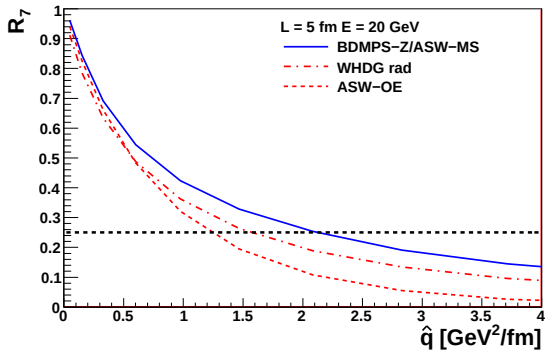

(b) $L = 5$ fm.

FIG. 19: Correlation between R_7 and $\hat{q}$ for a primary quark with $E = 20$ GeV for different energy loss formalisms. The horizontal black dashed line indicates $R_7 = 0.25$.

$R_7 = 0.25$		T (MeV)	$\hat{q}$ (GeV^2/fm)	ω_c or $\bar{\omega}_c L/\lambda$ (GeV)	R or $\bar{R}L/\lambda$	L/λ	$m_{\rm D}$ (GeV)
$L = 2$ fm	ASW–MS	1030	23.2	236	2393	—	—
	WHDG	936	17.8	105	1063	6.25	1.82
	ASW–SH	727	8.86	49.0	500	4.85	1.41
	AMY	480	2.7	—	—	—	—
$L = 5$ fm	ASW–MS	434	2.11	134	3401	—	—
	WHDG	358	1.23	36.5	925	5.97	0.69
	ASW–SH	326	0.95	27.6	702	5.44	0.63
	AMY	235	0.4	—	—	—	—

TABLE II: Values of the model parameters required to reach the typical suppression of $R_7 = 0.25$.

tings are included. In the AMY formalism it is not possible to distinguish between thermal and radiated gluons for $\omega < 2$ GeV which is why in this region for AMY the gluon spectrum is not shown. We note that the ASW–MS single gluon spectrum at fixed suppression is harder than that obtained in the opacity expansions.

Figure 21 shows the final quark energy spectrum as function of $z_E = 1 - \epsilon$ for the two bricks of different lengths and $R_7 = 0.25$. The probability that a parton is absorbed in the medium is indicated by the squares at $z_{\rm E} = 0$. In this case the parton loses more energy than it initially has and gets absorbed in the medium. This happens if the energies of the multiple radiated gluons adds up to a total energy loss that exceed the initial energy of the parent parton. Since in WHDG radiative there is a large x cut-off, this probability is smaller than in ASW–MS and ASW–SH. The corresponding probability for losing no energy at all, a discrete weight for all models, is given by the squares at $z_{\rm E} = 1$.

The discrete and the absorption probabilities of the multiple-soft scattering approximation are larger than for the opacity expansions. It seems that the continuous part of the energy loss probability distribution is more relevant in the opacity expansion.

In the AMY energy loss kernel a lot of soft gluons are radiated which is consistent with the gluon distribution in Fig. 20. In the final quark spectrum a peak at $z_{\rm E} = 0.9$ is observed for AMY which corresponds to one radiated gluon of 2 GeV or to multiple gluons of energies lower than 2 GeV. The latter is most likely the case, but it falls into the region where we cannot distinguish the radiated gluons from the thermal gluons in the AMY formalism.

When all the models are tuned to a fixed amount of suppression R_7, the radiated gluon spectra look different. From the single gluon radiation spectra shown in Fig. 20 the average number of emitted gluons can be obtained by integrating the gluon spectrum over the gluon energy ω:

$$\langle N_g \rangle = \int d\omega \frac{dI}{d\omega}. \tag{B3}$$

Note that this determines the discrete weight of the probability for no energy loss:

$$p_0 = e^{-\langle N_g \rangle}. \tag{B4}$$

The probability for complete absorption of the parton is then given by

$$p_1 = \int_E^\infty d(\Delta E)\, P(\Delta E), \tag{B5}$$

where E is the energy with which the parent parton enters the brick. The total average energy loss for the in-

		$T = 300$ MeV				$R_7 =$ 0.25			
		$\langle N_g \rangle$	$\langle \Delta E \rangle$	p_0	p_1	$\langle N_g \rangle$	$\langle \Delta E \rangle$	p_0	p_1
$L = 2$ fm	ASW–MS	0.17	0.3	0.84	0.01	1.58	5.9	0.2	0.46
	WHDG	0.48	1.24	0.62	0.00	1.94	7.7	0.14	0.14
	ASW–SH	0.25	0.93	0.78	0.03	1.92	6.9	0.15	0.35
$L = 5$ fm	ASW–MS	0.12	3.95	0.31	0.08	1.83	6.4	0.16	0.33
	WHDG	1.96	5.63	0.14	0.05	2.44	7.3	0.09	0.11
	ASW–SH	2.09	5.76	0.12	0.2	2.47	6.7	0.08	0.26

TABLE III: Table of different variables for the different energy loss models. Left columns: for $T = 300$ MeV for all models. Right columns: corresponding medium properites required to reach the typical suppression $R_7 = 0.25$.

coming parton is calculated from the energy loss probability distribution $P(\Delta E)$:

$$\langle \Delta E \rangle = \int_0^E d(\Delta E)\ P(\Delta E), \tag{B6}$$

for which only the surviving partons are taken into account.

All the mentioned values characterizing the different models are listed in Table III. The Table shows that the same suppression factor R_7 does not imply that the mean energy loss is the same for all models. We also note that the number of radiated gluons differs significantly between the models at fixed temperature. On the other hand, when the suppression factor R_7 is fixed, the number of radiated gluons is similar.

d. *Correlation of $\hat{q}$ and L*

Figure 22 shows contours for different suppression factors R_7 as function of the in-medium path length L and the transport coefficient $\hat{q}$. Since the typical size of a nucleus is $L \approx 5$ fm, the relevant path lengths are $L \lesssim 5$. In this region a relatively small difference in L results in a very large difference in $\hat{q}$ for a fixed value of R_7. A rescaling in L is much more efficient than a rescaling in the medium density because the energy loss scales with $\hat{q}L^2$. To achieve a significant difference in the fraction of lost energy a large step in medium density is needed.

The WHDG radiative model requires larger combinations of $\hat{q}$ and L than ASW–SH in order to achieve the same suppression factor. This is due to the smooth cutoff in the single gluon spectrum at the quark energy ($E = 20$ GeV) in the WHDG model, cf. Fig. 19. For small $\hat{q}$ and small L this is not a dominant effect because the tail of the single gluon energy distribution is shorter which makes the single gluon spectra of ASW–SH and WHDG and thus the energy loss probability distribution less different. This is also represented in the crossing points at small $\hat{q}$ of the two opacity expansion curves in Fig. 19.

The multiple soft scattering approximation requires larger values for $\hat{q}$ and L than both opacity expansion formalisms in order to achieve the same fraction of energy loss. The region in $\hat{q}$ and L in which a parton survives is more limited for the opacity expansion than for the multiple soft scattering approximation. This is mainly due to the larger probability for losing no energy in the multiple-soft approximation at the same medium density.

[1] K. Adcox et al. (PHENIX), Phys. Rev. Lett. **88**, 022301 (2002), nucl-ex/0109003.
[2] C. Adler et al. (STAR), Phys. Rev. Lett. **89**, 202301 (2002), nucl-ex/0206011.
[3] M. H. Thoma, Phys. Lett. **B273**, 128 (1991).
[4] M. G. Mustafa and M. H. Thoma, Acta Phys. Hung. **A22**, 93 (2005), hep-ph/0311168.
[5] M. Gyulassy and X.-n. Wang, Nucl. Phys. **B420**, 583 (1994), nucl-th/9306003.
[6] R. Baier, Y. L. Dokshitzer, A. H. Mueller, S. Peigne, and D. Schiff, Nucl. Phys. **B483**, 291 (1997), hep-ph/9607355.
[7] R. Baier, D. Schiff, and B. G. Zakharov, Ann. Rev. Nucl. Part. Sci. **50**, 37 (2000), hep-ph/0002198.
[8] U. A. Wiedemann (2009), 0908.2306.
[9] A. Majumder and M. Van Leeuwen (2010), 1002.2206.
[10] S. A. Bass et al., Phys. Rev. **C79**, 024901 (2009), 0808.0908.
[11] M. Gyulassy, I. Vitev, X.-N. Wang, and B.-W. Zhang (2003), nucl-th/0302077.
[12] D. d'Enterria (2009), 0902.2011.
[13] R. Baier, Y. L. Dokshitzer, A. H. Mueller, and D. Schiff, Nucl. Phys. **B531**, 403 (1998), hep-ph/9804212.
[14] B. G. Zakharov, JETP Lett. **63**, 952 (1996), hep-ph/9607440.
[15] U. A. Wiedemann, Nucl. Phys. **B588**, 303 (2000), hep-ph/0005129.
[16] M. Gyulassy, P. Levai, and I. Vitev, Nucl. Phys. **B571**, 197 (2000), hep-ph/9907461.
[17] M. Gyulassy, P. Levai, and I. Vitev, Nucl. Phys. **B594**, 371 (2001), nucl-th/0006010.
[18] M. Gyulassy, P. Levai, and I. Vitev, Phys. Lett. **B538**,

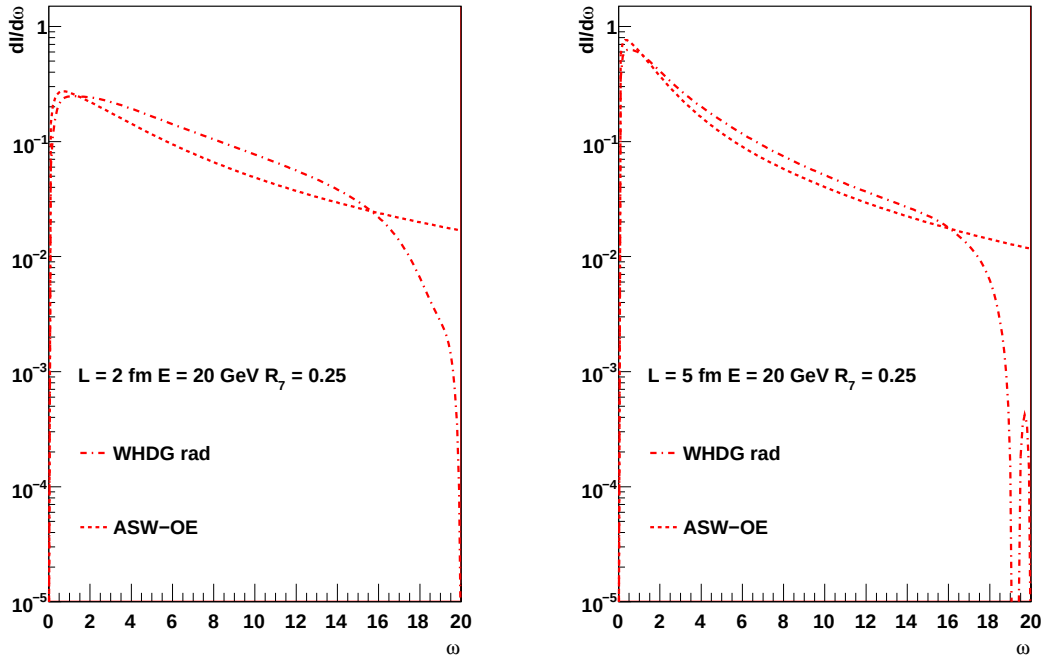

FIG. 20: The inclusive gluon spectrum for quarks with $E = 20$ GeV and for path-lengths $L = 2$ fm (left panel) and $L = 5$ fm (right panel)..

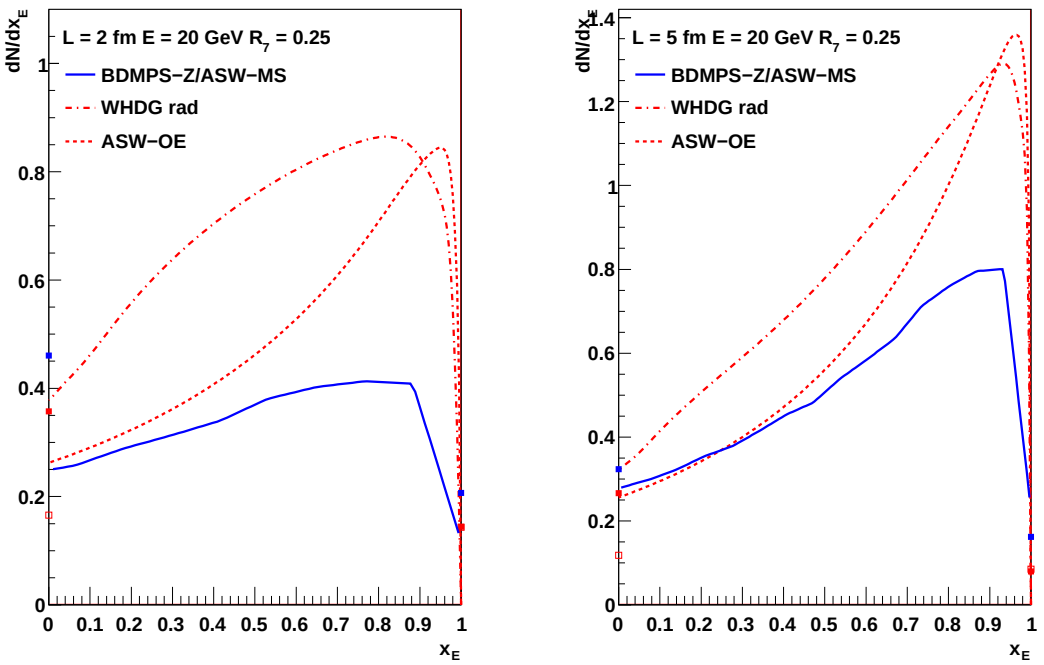

FIG. 21: The final quark energy spectra as function of $z_{\rm E} = 1 - \epsilon$ and for path-lengths $L = 2$ fm (left panel) and $L = 5$ fm (right panel). All models are scaled to the same suppression $R_7 = 0.25$. The squares at $z_{\rm E} = 0$ indicate the probability that a quark is absorbed and at $z_{\rm E} = 1$ the probability that a quark does not interact with the medium. Solid blue squares: BDMPS-Z/ASW–MS. Open red squares: WHDG rad. Solid red squares: ASW–SH.

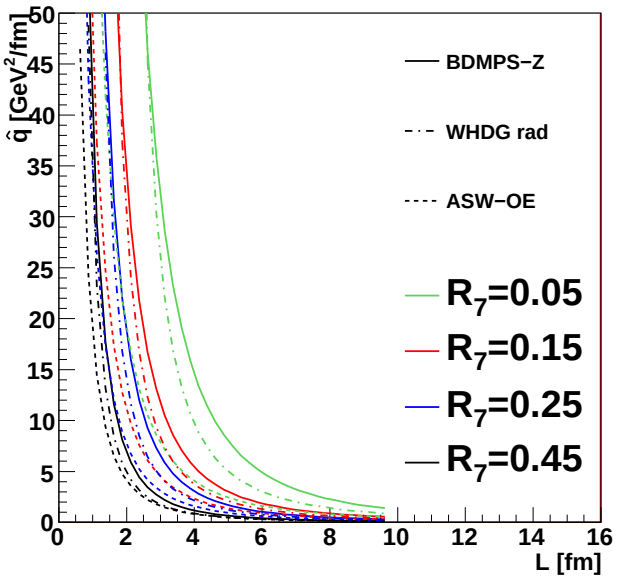

FIG. 22: Transport coefficent as function of in-medium path length for BDMPS-Z/ASW-MS (solid lines), WHDG radiative (dashed dotted lines) and ASW-SH (dashed lines) energy loss models. The lines represent isolines from brick calculations for $R_7 = 0.05$ (green), 0.15 (red), 0.25 (blue) and 0.45 (black). This is for quarks with $E = 20$ GeV.

282 (2002), nucl-th/0112071.
[19] S. Wicks (2008), 0804.4704.
[20] P. B. Arnold, Phys. Rev. **D80**, 025004 (2009), 0903.1081.
[21] S. Wicks, W. Horowitz, M. Djordjevic, and M. Gyulassy, Nucl. Phys. **A784**, 426 (2007), nucl-th/0512076.
[22] M. Djordjevic and U. W. Heinz, Phys. Rev. Lett. **101**, 022302 (2008), 0802.1230.
[23] X.-N. Wang and X.-f. Guo, Nucl. Phys. **A696**, 788 (2001), hep-ph/0102230.
[24] A. Majumder (2009), 0901.4516.
[25] P. B. Arnold, G. D. Moore, and L. G. Yaffe, JHEP **12**, 009 (2001), hep-ph/0111107.
[26] P. B. Arnold, G. D. Moore, and L. G. Yaffe, JHEP **06**, 030 (2002), hep-ph/0204343.
[27] U. A. Wiedemann, Nucl. Phys. **A690**, 731 (2001), hep-ph/0008241.
[28] W. A. Horowitz and B. A. Cole, Phys. Rev. **C81**, 024909 (2010), 0910.1823.
[29] S. Wicks (2008), ph.D thesis Columbia University, URL `http://proquest.umi.com/pqdweb?sid=1&Fmt=2&clientId=79356&RQT%=309&VName=PQD&did=1614268891`.
[30] P. Arnold, Phys. Rev. **D79**, 065025 (2009), 0808.2767.
[31] S. Caron-Huot and C. Gale (2010), 1006.2379.
[32] P. B. Arnold and W. Xiao, Phys. Rev. **D78**, 125008 (2008), 0810.1026.
[33] S. Caron-Huot, Phys. Rev. **D79**, 065039 (2009), 0811.1603.
[34] A. Majumder and B. Muller, Phys. Rev. **C77**, 054903 (2008), 0705.1147.
[35] M. Djordjevic and M. Gyulassy, Nucl. Phys. **A733**, 265 (2004), nucl-th/0310076.
[36] N. Armesto, C. A. Salgado, and U. A. Wiedemann (2004), hep-ph/0405184.
[37] N. Armesto, C. A. Salgado, and U. A. Wiedemann, Phys. Rev. **D69**, 114003 (2004), hep-ph/0312106.
[38] M. Djordjevic, Phys. Rev. **C80**, 064909 (2009), 0903.4591.
[39] C. A. Salgado and U. A. Wiedemann, Phys. Rev. **D68**, 014008 (2003), hep-ph/0302184.
[40] N. Armesto, L. Cunqueiro, C. A. Salgado, and W.-C. Xiang, JHEP **02**, 048 (2008), 0710.3073.
[41] K. Zapp, G. Ingelman, J. Rathsman, J. Stachel, and U. A. Wiedemann, Eur. Phys. J. **C60**, 617 (2009), 0804.3568.
[42] K. Zapp, J. Stachel, and U. A. Wiedemann, Phys. Rev. Lett. **103**, 152302 (2009), 0812.3888.
[43] N. Armesto, L. Cunqueiro, and C. A. Salgado, Eur. Phys. J. **C63**, 679 (2009), 0907.1014.
[44] N. Armesto, G. Corcella, L. Cunqueiro, and C. A. Salgado, JHEP **11**, 122 (2009), 0909.5118.
[45] K. J. Eskola, H. Honkanen, C. A. Salgado, and U. A. Wiedemann, Nucl. Phys. **A747**, 511 (2005), hep-ph/0406319.
[46] A. Dainese, C. Loizides, and G. Paic, Eur. Phys. J. **C38**, 461 (2005), hep-ph/0406201.
[47] T. Renk and K. Eskola, Phys. Rev. **C75**, 054910 (2007), hep-ph/0610059.
[48] T. Renk, J. Ruppert, C. Nonaka, and S. A. Bass, Phys. Rev. **C75**, 031902 (2007), nucl-th/0611027.
[49] N. Armesto, M. Cacciari, T. Hirano, J. L. Nagle, and C. A. Salgado (2009), 0907.0667.
[50] R. Baier, Y. L. Dokshitzer, A. H. Mueller, S. Peigne, and D. Schiff, Nucl. Phys. **B484**, 265 (1997), hep-ph/9608322.
[51] B. G. Zakharov, JETP Lett. **65**, 615 (1997), hep-ph/9704255.
[52] P. B. Arnold, G. D. Moore, and L. G. Yaffe, JHEP **11**, 057 (2001), hep-ph/0109064.
[53] S. Jeon and G. D. Moore, Phys. Rev. **C71**, 034901 (2005), hep-ph/0309332.
[54] E. Braaten and R. D. Pisarski, Phys. Rev. Lett. **64**, 1338 (1990).
[55] E. Braaten and R. D. Pisarski, Nucl. Phys. **B337**, 569 (1990).
[56] G.-Y. Qin et al., Phys. Rev. Lett. **100**, 072301 (2008), 0710.0605.
[57] B. Schenke, C. Gale, and G.-Y. Qin, Phys. Rev. **C79**, 054908 (2009), 0901.3498.
[58] J. Adams et al. (STAR), Phys. Lett. **B637**, 161 (2006), nucl-ex/0601033.
[59] J. Adams et al. (STAR), Phys. Rev. Lett. **91**, 172302 (2003), nucl-ex/0305015.
[60] S. S. Adler et al. (PHENIX), Phys. Rev. Lett. **91**, 072301 (2003), nucl-ex/0304022.
[61] S. S. Adler et al. (PHENIX), Phys. Rev. **C69**, 034910 (2004), nucl-ex/0308006.
[62] We note that the ASW–SH implementation [39] is only in terms of the Poisson convoluted energy loss probability distribution, which we will discuss in detail further below. The comparison shown here was obtained from an independent numerical implementation of the massless ASW–SH formula by B. Cole that well reproduces the Poisson convolution results of [39].
[63] In GLV and BDMPS (4) is used to neglect poles from

propagators multiplied by $\exp(-\mu\Delta z) \approx \exp(-\mu\lambda) \ll 1$, where Δz is the distance between successive scattering centers; this approach is probably invalid for $L \lesssim \lambda \sim 1$ fm. On the other hand AMY uses the central limit theorem in its Langevin approach and corrections are likely for $L \lesssim 30\lambda \sim 30$ fm; this extra long path length is also required by the neglect of the interference between vacuum and in-medium induced radiation.